Journal of Controlled Release 383 (2025) 113857

Contents lists available at ScienceDirect

Journal of Controlled Release

journal homepage: www.elsevier.com/locate/jconrel

A combinatorial siRNA and mRNA approach for obesity treatment using targeting lipid nanoparticles

William Stewart [a], Bin Hu [b], Fengqiao Li [a], Jia Huang [b], Zhixiang Liu [a], Chenshuang Zhang [b], Maoping Tang [b], Xue-Qing Zhang [c,*], Xiaoyang Xu [a,c,*]

[a] Department of Chemical and Materials Engineering, New Jersey Institute of Technology, Newark, NJ 07102, USA
[b] Shanghai Frontiers Science Center of Drug Target Identification and Delivery, School of Pharmaceutical Sciences, National Key Laboratory of Innovative Immunotherapy, Shanghai Jiao Tong University, Shanghai 200240, PR China
[c] Department of Biomedical Engineering, New Jersey Institute of Technology, Newark, NJ 07102, USA

ARTICLE INFO

Keywords:
Lipid nanoparticles
Targeted delivery
Obesity
Metabolic dysfunction
mRNA and siRNA mediated therapy

ABSTRACT

Obesity, a widespread global health issue affecting millions, is characterized by excess fat deposition and metabolic dysfunction, significantly elevating the risk of comorbidities like type 2 diabetes, cardiovascular disease, and certain cancers, all of which contribute to rising rates of preventable morbidity and mortality. Current approaches to obesity, including lifestyle modifications, and pharmacotherapy, often face limitations such as poor long-term adherence, side effects, and insufficient targeting of the complex, multifactorial pathways underlying the disease. Herein we report a dual, RNA-mediated combinatorial approach using targeting lipid nanoparticles (LNP) for the treatment of obesity. LNPs were co-encapsulated with mRNA encoding Interleukin-27 (*mIL-27*) to coactivate PGC-1α, PPARα, and UCP-1, thereby promoting adipocyte differentiation and enhancing adaptive thermogenesis within adipocytes, and siRNA targeting Dipeptidyl peptidase-4 (*siDPP-4*) to silence the primary inhibitory enzyme of GLP-1, and GIP within the incretin system, effectively restoring glucose homeostasis. Following post translational silencing of DPP-4 and upregulation of IL-27 in a diet-induced obesity (DIO) mice model, increased expression of thermogenic biomarkers PGC-1α, PPARα, and UCP-1 was observed at the molecular, protein, and tissue level, and insulin sensitivity was restored. Importantly, this gene modulation led to a 21.1 % reduction of bodyweight after treatment in the DIO model. These findings demonstrate for the first time a dual RNA-mediated combinatorial approach, leveraging liver targeting LNP delivery with synergistic effects from incretin system regulation and induction of adipocyte differentiation and thermogenesis after codelivery of *siDPP-4* and *mIL-27*. This innovative strategy provides a promising alternate framework for addressing obesity and its associated metabolic dysfunction.

1. Introduction

Obesity has emerged as a major global health crisis, affecting over 40 % of U.S. adults in 2023, and is a complex, multifactorial disease characterized by excessive adiposity and metabolic dysfunction [1–3]. Development of obesity leads to significantly increased risk of comorbidities such as type 2 diabetes, cardiovascular disease, and certain cancers, all of which contribute to rising global morbidity and mortality rates [1,4–6]. Recent advances in pharmacotherapies targeting the incretin system have resulted in novel treatment options for obesity, as exemplified by the GLP-1 receptor agonists Ozempic® and Mounjaro® [7–11]. This enhanced incretin system stimulation is demonstrated to reduce bodyweight significantly by promoting interactions in the hypothalamic satiety centers at the axis of the central nervous system and improving insulinotropic activity via incretin-mediated cAMP signaling, and subsequent stimulation of pancreatic b-cell function and glycolytic activity [7–10]. The development of dual and triple agonists, such as Tirzepitide and Retatrutide, aims to further amplify incretin responses by targeting GLP-1, GIP, and glucagon receptors to yield complementary insulinotropic effects [12–15]. However, despite these advancements, obesity remains a persistent challenge, and approximately 15 % of patients experience suboptimal therapeutic responses to GLP-1 receptor agonists [4]. Furthermore, targeting receptors exclusively within the incretin system can lead to more complex and potentially severe side

* Corresponding authors at: Department of Biomedical Engineering, New Jersey Institute of Technology, Newark, NJ 07102, USA.
E-mail addresses: xueqingzhang@sjtu.edu.cn (X.-Q. Zhang), xiaoyang.xu@njit.edu (X. Xu).

https://doi.org/10.1016/j.jconrel.2025.113857
Received 11 March 2025; Received in revised form 10 May 2025; Accepted 15 May 2025
Available online 16 May 2025

effects. While clinical studies have reported significant weight loss effects, separate studies have found that lean muscle mass accounted for up to 39 % and 41 % of the total weight loss [11,13–18]. This variability in therapeutic response, and non-selective weight loss underscores the need for alternative strategies to more effectively address the obesity epidemic. Integrating approaches that target enhanced energy expenditure, in combination with incretin-based mechanisms, may offer a more comprehensive and effective approach to obesity management, ultimately leading to improved clinical outcomes by rebalancing metabolic activity.

Herein, we propose a novel approach utilizing cellular targeting lipid nanoparticle (LNP) technology to deliver RNA-based therapeutics for the treatment of obesity and metabolic dysfunction. This dual-modality strategy combines messenger RNA (mRNA) protein therapy with RNA interference (RNAi) to modulate alternate metabolic pathways and address the efficacy limitation of current treatments. Specifically, this approach leverages hepatocyte-targeting LNPs, prepared by surface modification with *N*-acetylgalactosamine (GalNAc) to enable

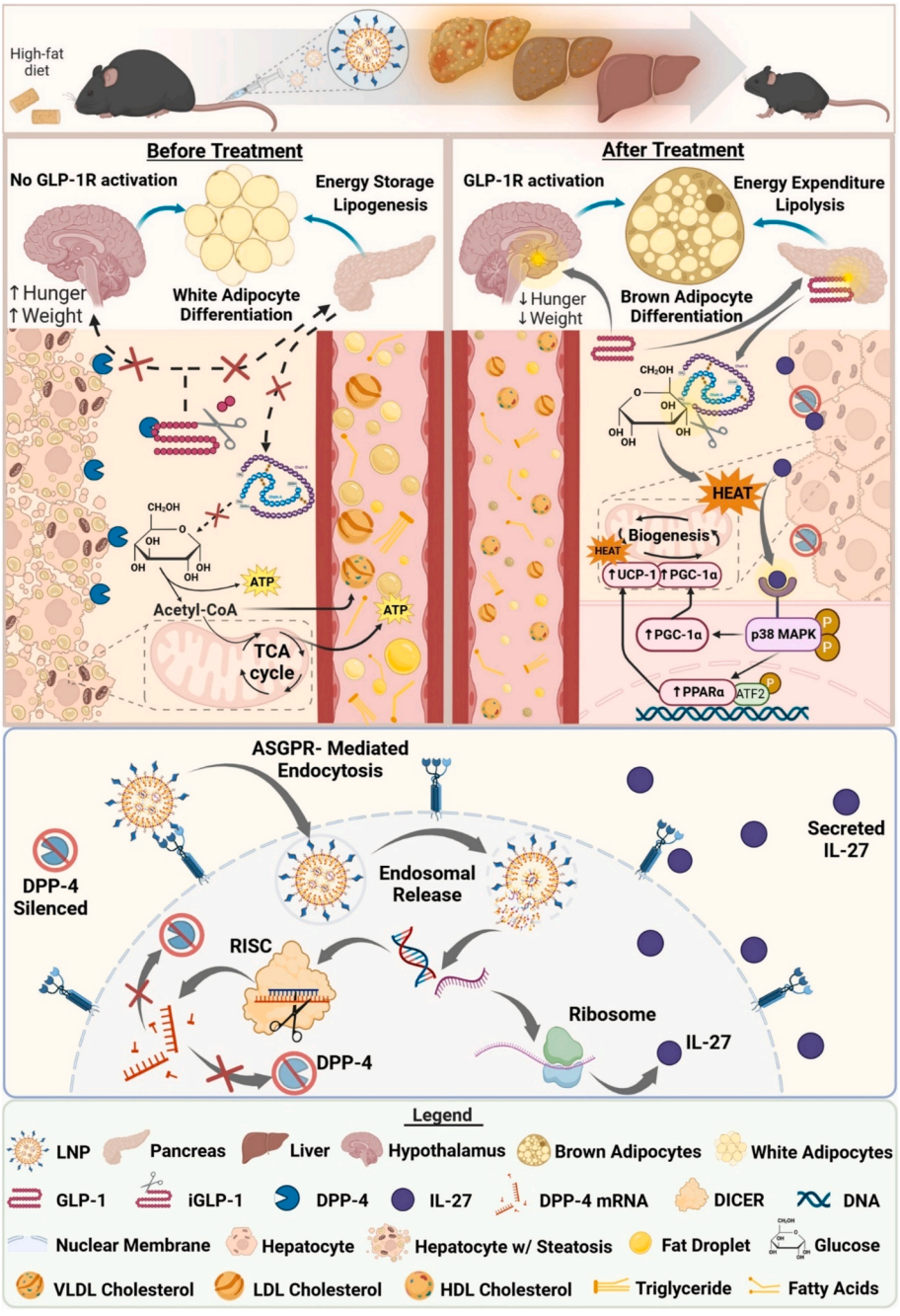

Fig. 1. Schematic representation of reduction of bodyweight after treatment with *@LNP-GNc* and *@LNP* containing *siDPP-4* and *mIL-27*. B) Schematic representation of IL-27 and DPP-4 mediated processes for stimulation of insulinotropic activity, adipocyte differentiation and adaptive thermogenesis. Post translational gene silencing of DPP-4 reduces circulating concentrations of DPP-4, resulting in decreased GLP-1 and GIP inhibition by enzymatic cleavage, and prolonged receptor stimulation and incretin system activation to improve insulinotropic and glycolytic activity. Enhanced hepatic secretion of IL-27 activates P38MAPK-PGC-1α signaling pathway, resulting in activation of key thermogenic coregulators PGC-1α, PPARα, and UCP-1 which generate a synergistic effect in promoting white-to-brown adipocyte differentiation, and stimulating adaptive thermogenesis in newly formed and existing brown adipocytes. (For interpretation of the references to colour in this figure legend, the reader is referred to the web version of this article.)

Asialoglycoprotein receptor (ASGPR)-mediated uptake [19–22]. Improvements to hepatocyte targeted delivery serves a dual purpose in simultaneously optimizing the therapeutic response while minimizing off-target effects. The mRNA encodes interleukin-27 (IL-27), a hepatocyte secreted protein, which activates the P38MAPK-PGC-1α signaling pathway to promote coactivation of peroxisome proliferator-activated receptor gamma coactivator 1-alpha (PGC-1α), peroxisome proliferator-activated receptor alpha (PPARα), and uncoupling protein-1 (UCP-1), three key transcriptional regulators involved in mitochondrial biogenesis, oxidative metabolism, and differentiation of adipocytes for thermogenesis [23–30]. Concurrently, post translational gene silencing of Dipeptidyl peptidase-4 (DPP-4) reduces circulating DPP-4 concentration, thereby reducing enzymatic inhibition of endogenous GLP-1, and resulting in cascading insulinotropic and glycolytic effects from prolonged activation GLP-1 and GIP receptors, enhanced cAMP signaling, and improved pancreatic b-cell function [8,11,31–33] (See Fig. 1). Together, this orthogonal mechanistic approach is hypothesized to generate a synergistic effect in addressing energy balance by reducing energy intake through the resensitization of the incretin system to glucose stimuli while simultaneously increasing adipocyte specific energy expenditure by promoting adipose tissue differentiation and thermogenesis.

A surface modified LNP was prepared by conjugating GalNAc to DMG-PEG, prior to self-assembly in a microfluidic device and resulted in ~90 nm particles, with polydispersity indices below 0.2, and encapsulation efficiencies in excess of 90 %. In vitro evaluation of GalNAc LNPs containing either *mIL-27* or *siDPP-4* resulted in improved protein expression or gene knockdown in Hepa 1–6 cells compared to non-targeting LNPs, as determined by qPCR. Additionally, in vivo evaluation of targeting LNPs encapsulating Luciferase mRNA demonstrated enhanced hepatic delivery compared to non-targeting LNPs. Preclinical evaluation using diet-induced obesity (DIO) mice models demonstrated that GalNAc-modified LNPs, encapsulating both *mIL-27* and *siDPP-4*, lead to a 21.1 % reduction in body weight over three weeks of treatment, along with significant improvements to biomarkers of metabolic health, including cholesterol, triglycerides, and blood glucose, and upregulation of the thermogenic biomarkers PGC-1α, PPARα, and UCP-1. Additionally, histological analysis of liver and adipose tissues indicates significant decreases in macrovesicular steatosis within hepatocytes, morphological reduction of adipocytes, and increases in cytoplasmic concentrations of UCP-1, the key indicator of brown adipocyte thermogenesis [34–36]. The combined RNA therapy also outperformed individual RNA treatments and nontargeting LNP delivery by as high as 13.6 %, highlighting the synergistic benefits of the targeted and combinatorial approach. This study presents a novel precision medicine strategy that combines dual RNA-based therapeutics with an advanced, targeted LNP delivery system for the treatment of obesity and metabolic dysfunction. By leveraging complementary mechanisms of action to enhance energy expenditure and regulate glucose homeostasis, this strategy provides an alternate framework to address critical gaps in existing pharmacotherapies and expands the obesity treatment paradigm beyond incretin-based interventions.

2. Results

2.1. Synthesis, characterization, and optimization of GalNAc-LNPs (@LNP-GNc)

Non-targeting LNPs (*@LNP*) were prepared using a previously reported optimized lipid composition of AA3-Dlin, DSPC, Cholesterol, and DMG-PEG at molar ratios of 40:10:47.5:1.5 [37]. Surface modified hepatocyte targeting LNPs (*@LNP-GNc*) were prepared by incorporating DMG-PEG-GalNAc prior to LNP self-assembly. Both *@LNP-GNc* and *@LNP* formulations demonstrated consistent particle sizes (~88–97 nm), low polydispersity (0.06–0.150), and high encapsulation efficiency (>95 %), irrespective of the RNA payloads (Fig. 2A). The incorporation of GalNAc onto the surface of LNPs increased the particle size by around 10 nm, although this difference is not thought to be significant, within the context of biological applications. Particle size and morphology were also confirmed by scanning electron microscopy to demonstrate a monodisperse population of smooth, spherical particles well below 200 nm (Fig. 2B).

2.2. In vitro evaluation of siDPP-4, mIL-27, @LNP and @LNP-GNc

To evaluate cellular internalization in vitro, both *@LNP-GNc* and *@LNP* were formulated with FITC labeled cholesterol, and incubated in Hepa1–6 cells for 4 h prior to fluorescence microscopy and flow cytometry analysis. FACS analysis indicates a higher degree of cellular internalization for the *@LNP-GNc* compared to the *@LNP* at 0.5, 2, and 4 h (Fig. 2G). Furthermore, cells treated with the targeted *@LNP-GNc* displayed a much higher fluorescence signal intensity compared to those treated with the non-targeting LNP counterpart, *@LNP*. Increasing the molar percentage of GalNAc from 2.5 % up to 5 % further enhanced the cellular signaling intensity (Fig. 2F). These results suggest that incorporation of the targeting GalNAc functional group greatly enhances LNP internalization into hepatocyte cell cultures. We then explored the therapeutic efficacy of *siDPP-4* and *mIL-27* concentration in *@LNP-GNc* LNPs. *Post* translational gene silencing in Hepa1–6 cells was observed at *siDPP-4* concentrations greater or equal to 1.5 μg/mL, with a maximum RNA knockdown below 30 % observed at 2.0 μg/mL *siDPP-4* (Fig. 2D). *mIL-27* delivery by *@LNP-GNc* to Hepa1–6 cells demonstrated dose-dependent increases in protein expression, with a minimum concentration of 0.5 μg *mIL-27* necessary for increased IL-27 expression in western blots (Fig. 2E).

2.3. In vivo mRNA delivery efficiency of mLuc@LNP-GNc

To evaluate the in vivo transfection efficiency of *@LNP-GNc* and *@LNP* formulations, luciferase-encoding mRNA (*mLuc*) was encapsulated in *@LNP* and *@LNP-GNc* and administered intravenously into healthy C57BL/6 J mice at doses of 3 μg *mLuc* per mouse. Consistent with cellular uptake results, *mLuc@LNP-GNc* demonstrated improved translation and localization of luciferase into the liver compared to *mLuc@LNP*, with differences in bioluminescence seen as early as 12 h and as late as 48 h after injection, confirming improved hepatocyte targeting. The liver-specific expression increased as the percentage of incorporated GalNAc increased to 2.5 %, resulting in an average radiance of 7.96×10^8 p/s/cm^2/sr after 24 h, compared to 1.63×10^7 p/s/cm^2/sr for the non-targeting *mLuc@LNP* control group (Fig. 2C). Notably, an increased concentration of 5 % GalNAc produced a transient increase of 66 % in liver-specific luminescence intensity after 12 h, but diminished effects at 24 h and beyond, with an average radiance of 3.27×10^7 p/s/cm^2/sr (Fig. 2C). To further assess the liver-targeted biodistribution, *mLuc@LNP*, *mLUC@LNP-GNc$^{2.5\%}$*, *and mLuc@LNP-GNc$^{5\%}$* formulations were labeled with DiR fluorescent dye, prior to administration in C57BL/6 J mice are doses of 3 μg *mLuc* per mouse. Mice were euthanized 6 h post-injection and major organs were harvested for ex vivo fluorescent imaging (Fig. S6). LNPs modified with 2.5 % GalNAc exhibited enhanced liver accumulation and biodistribution compared to the unmodified LNPs, and LNPs modified with 5 % GalNAc. These results unequivocally highlight the role of GalNAc functionalization in surface modified *@LNP-GNc* to achieve precise hepatocyte targeting, enhancing mRNA delivery efficiency and accumulation.

2.4. siDPP4-mIL27@LNP-GNc induces robust gene silencing of DPP-4, and expression of IL-27 within hepatocytes

We next investigated the therapeutic efficacy of *siDPP4-mIL27@LNP-GNc* to treat obesity and reduce bodyweight in a DIO mice model. C57BL/6 J mice were fed exclusively on high-fat diet (60 % calories from fat) for 5 weeks prior to treatment and maintained on HFD during

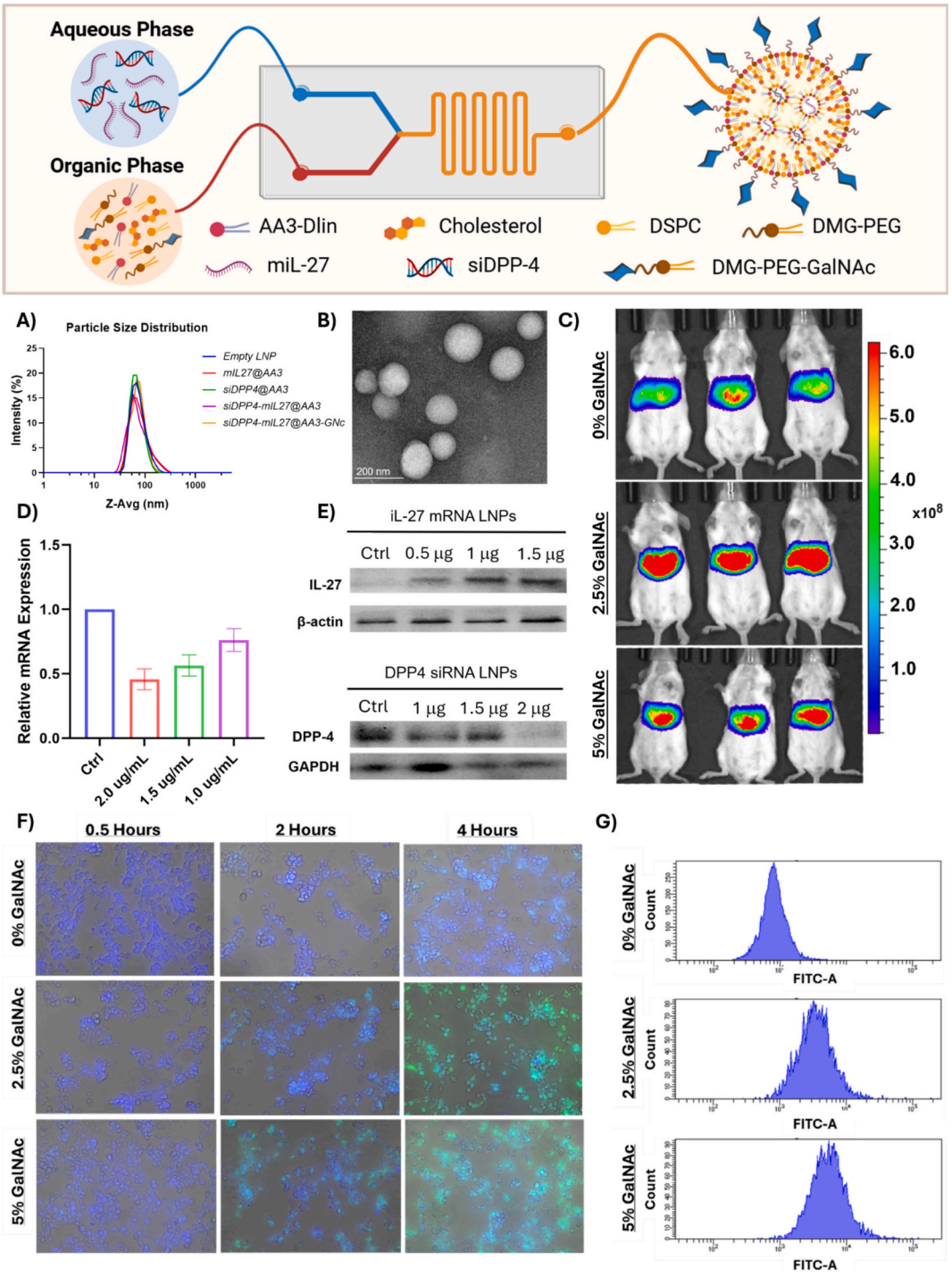

Fig. 2. Preparation, physical characterization, in vitro and in vivo evaluation of *mRNA@LNP-GNc* formulations. (A) Particle size distributions measured by dynamic light scattering (DLS). Hydrodynamic diameter measurement is reported as %intensity. (B) Representative Transmission Electron Microscopy (TEM) image of a *siDPP4-mIL27@LNP-GNc*, Scale bar 200 nm. (C) In vivo bioluminescence imaging of *mLuc@LNP-GNc* and *mLuc@LNP* after 24 h to determine optimized molar percentage of DMG-PEG-GalNAc (Radiance [(p/s)/(cm^2/sr)], 1.85e7 minimum, 6.6e8 maximum). (D) Dose effects of *siDPP-4* induced gene knockdown in Hepa1–6 cells. (E) Immunoblot evaluation for dose effects of *mIL-27* and *siDPP-4* delivered by *@LNP-GNc*. (F-G) Cellular uptake (F) and FACS (G) analysis demonstrate improved uptake of FITC labeled LNPs containing GalNAc in Hepa-1-6 cells after 4 h (merged fluorescence microscopy DAPI (blue) and FITC (green). (For interpretation of the references to colour in this figure legend, the reader is referred to the web version of this article.)

treatment to exacerbate obesity effects. Treatments containing individual RNA therapies, and combination therapies in both non-targeting and targeting LNPs were administered to evaluate both individual and synergistic effects of *siDPP-4* and *mIL-27*, in combination with enhanced hepatocyte specific delivery. Mice (n = 5) were treated biweekly via lateral tail vein injection with LNPs containing 15 µg of *mIL-27*, 15 µg *siDPP-4*, or both (0.4 mg/kg or 0.8 mg/kg total RNA), for a total of six treatments over 3 weeks. Body weight and food intake were monitored every 2–3 days during treatment. After six treatments, mice were weighed, sacrificed, and serum, organs, and fat tissues were collected for measurement.

To support the canonical extrahepatic modulation of the incretin

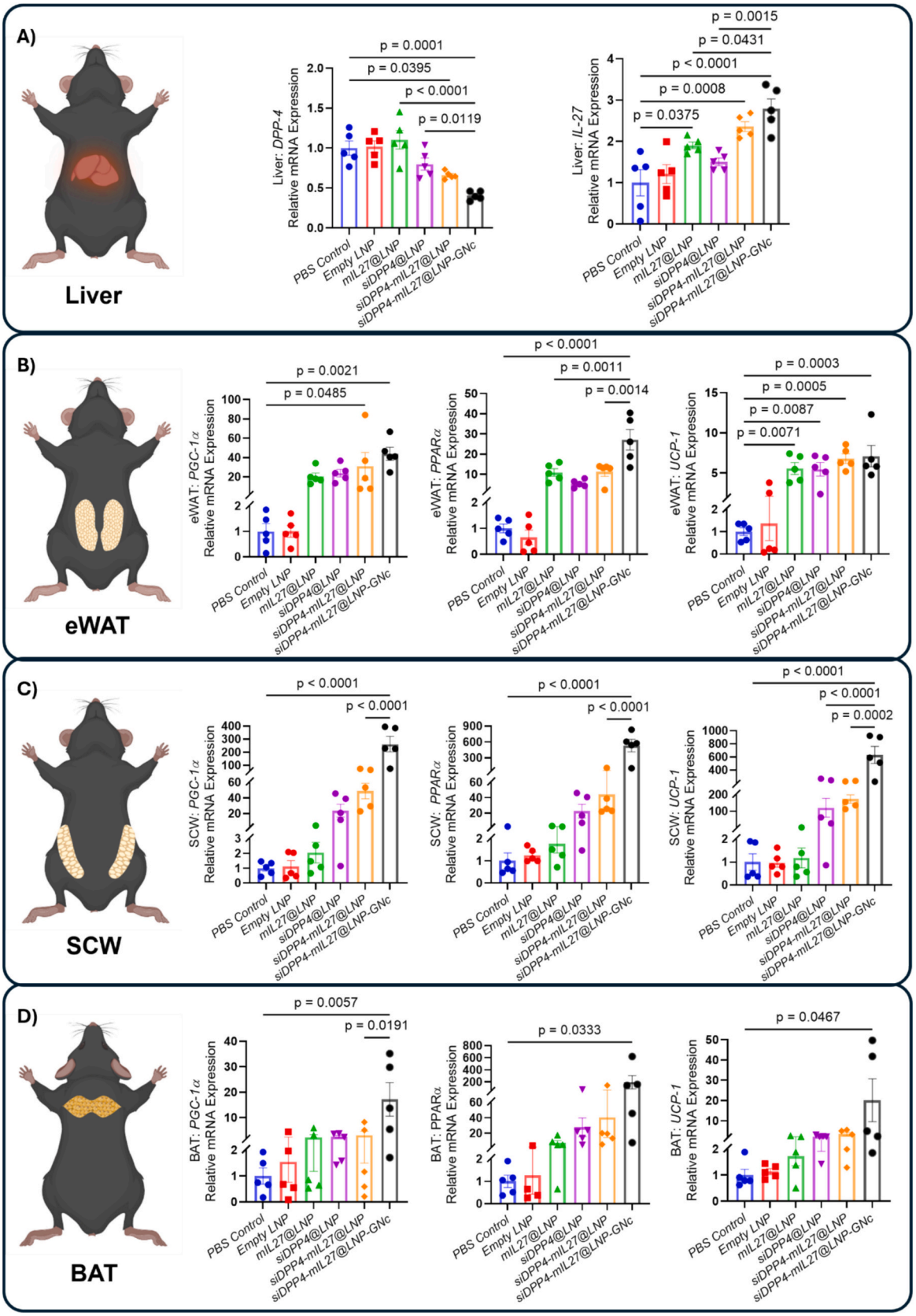

Fig. 3. *siDPP4-mIL27@LNP-GNc* downregulates DPP-4, and upregulates IL-27 expression in hepatocytes, stimulating canonical upregulation of the thermogenic coactivators PGC-1α, PPARα, and UCP-1 in eWAT, SCW, and BAT. (A) Relative expression levels of DPP-4 (left) and IL-27 (right) in liver homogenates of DIO mice treated with *siDPP4@LNP, mIL27@LNP, siDPP4-mIL27@LNP, siDPP4-mIL27@LNP-GNc* ($n = 5$). (B–D) Relative expression levels of PGC-1α (B), PPARα (C), and UCP-1 (D), in eWAT (left), SCW (middle), and BAT (right) (n = 5). Results are presented as means ± SEM, and statistical significance was assessed using one-way ANOVA with Tukey test.

system via post translation gene silencing of DPP-4, and IL-27 activation of the P38MPAK-PGC-1α signaling pathway to promote thermogenesis within adipocytes, it was critical to determine the concentrations of IL-27 and DPP-4 specifically within hepatocytes. Quantitative real-time polymerase chain reaction (qPCR) was conducted to analyze RNA expression levels of liver specific DPP-4 and IL-27 (Fig. 3 A). Treatment groups receiving *siDPP4-mIL27@LNP* and *siDPP4-mIL27@LNP-GNc* therapies showed significant downregulation of DPP-4 expression in liver tissue, with reductions of DPP-4 RNA totaling 34 %, and 60 %, respectively. Unsurprisingly, liver homogenates from all *mIL-27* containing treatment groups exhibited elevated IL-27 RNA expression, with 1.9-, 2.3-, and 2.8-fold increases in upregulation in the *mIL27@LNP, siDPP4-mIL27@LNP*, and *siDPP4-mIL27@LNP-GNc* groups, respectively (Fig. 3 A).

2.5. siDPP4-mIL27@LNP-GNc activates thermogenesis and adipocyte differentiation directly within adipose tissue

To provide mechanistic support underlying the significant weight reduction observed in the DIO mice model following *siDPP4-mIL27@LNP-GNc* treatment, we assessed the RNA expression levels of P38MAPK-PGC-1α pathway specific thermogenic markers PGC-1α, PPARα, and UCP-1 in hepatocytes, epididymal white adipose (eWAT), subcutaneous inguinal white adipose (SCW), and interscapular brown adipose (BAT) via qPCR. Consistent with expectations, *siDPP4-mIL27@LNP-GNc* treatment significantly upregulated PGC-1α expression in eWAT (Fig. 3B), SCW (Fig. 3C), and BAT (Fig. 3D) homogenates with respective increases of 44.5-, 270-, and 5.4-fold. Additionally, the non-targeting combinatorial *siDPP4-mIL27@LNP* treatment elevated eWAT PGC-1α by 30.9-fold (Fig. 3B). As a master regulator of adaptive thermogenesis, PGC-1α is central to stimulating adipocyte differentiation during coactivation with PPARα, and coregulating thermogenesis upon transcriptional induction of UCP-1 within the cellular mitochondria.

PPARα expression was significantly upregulated in eWAT by 10.8-, 11.1- and 27.1- fold after treatment with *mIL27@LNP*, *siDPP4-mIL27@LNP*, and *siDPP4-mIL27@LNP-GNc*, respectively (Fig. 3B). Moreover, SCW (Fig. 3C) and BAT (Fig. 3D) tissues demonstrated striking increases of 529- and 195-fold in PPARα expression after *siDPP4-mIL27@LNP-GNc* treatment. Activation of PPARα promotes preadipocyte differentiation into mature adipocytes, induces adiponectin expression for enhanced lipid metabolism, and coregulates transcriptional activation of UCP-1 to drive mitochondrial biogenesis.

The expression of UCP-1, the key thermogenic activator in brown and beige adipocytes, was significantly upregulated in eWAT by 5.4-, 5.5-, 6.8-, and 7.2-fold following *siDPP4@LNP, mIL27@LNP siDPP4-mIL27@LN*, and *siDPP4-mIL27@LNP-GNc* treatments, respectively (Fig. 3B). SCW (Fig. 3C) and BAT (Fig. 3D) tissues demonstrated remarkable increases in UCP-1 expression, with 640- and 20-fold upregulation observed after *siDPP4-mIL27@LNP-GNc* treatment. These findings highlight a robust enhancement of metabolic energy expenditure and adaptive thermogenesis driven by the activation of UCP-1, an exclusive hallmark of brown and beige adipocyte function. Collectively, the coordinated upregulation of PGC-1α, PPARα, and UCP-1 underpins enhanced thermogenesis, mitochondrial activity, and adipocyte differentiation that contribute to the observed weight reduction and improvements to metabolic health. This mechanistic insight reinforces the therapeutic potential of *siDPP4-mIL27@LNP-GNc* in combating obesity and its associated metabolic disorders.

2.6. siDPP4-mIL27@LNP-GNc modulates protein expression of IL-27, DPP-4, and thermogenic biomarkers in liver and adipose tissue

To complement the observed RNA-level changes, we next evaluated whether *siDPP4-mIL27@LNP-GNc* effectively translates these transcriptional modulations into corresponding protein-level alterations for the key metabolic and thermogenic markers in liver and adipose tissues.

Western blot analyses revealed the highest protein concentrations of PGC-1α, PPARα, UCP-1, and IL-27 in *siDPP4-mIL27@LNP-GNc*-treated tissues, with progressively lower levels in *siDPP4-mIL27@LNP, mIL27@LNP,* and *siDPP4@LNP* groups. In contrast, DPP-4 protein levels were inversely correlated, with *siDPP4-mIL27@LNP-GNc* showing the most significant reduction, followed by *siDPP4-mIL27@LNP, mIL27@LNP* and *siDPP4@LNP (*Fig. 4 A).

These results underscore the efficacy of *siDPP-4* and *mIL-27*-containing LNPs in mediating targeted gene silencing and upregulation of pathways critical for thermogenesis and metabolic regulation. By effectively modulating protein expression in liver and adipose tissues, *siDPP4-mIL27@LNP-GNc* activates key cellular signaling pathways, offering a robust mechanistic basis for its potential to counteract obesity and associated metabolic dysregulation.

2.7. siDPP4-mIL27@LNP-GNc reduces obesity and adipose tissue mass in DIO model

At the conclusion of the six treatments, mice bodyweights (Fig. 5B), Food intake (Fig. 7 A) and adipose tissue deposits (Fig. 5D) were collected and measured to determine the impact of RNA based treatments in the DIO murine model. *siDPP4-mIL27@LNP-GNc* treatment achieved the greatest reduction in bodyweight (21.1 %), followed by *siDPP4-mIL27@LNP* (17.4 %), *mIL27@LNP* (17.2 %), and *siDPP-4@LNP* (8.9 %), compared to PBS controls. In contrast, PBS and empty LNP control groups gained ~11 % bodyweight, further demonstrating the significant weight reduction benefit from *mIL-27* and *siDPP-4* delivered by *@LNP* and *@LNP-GNc*.

Adipose tissue-specific analysis confirmed the superiority of targeted delivery of the combinatorial therapeutic. While all RNA treatments reduced individual fat deposits and total fat mass, the greatest effect was seen in *siDPP4-mIL27@LNP-GNc* treated mice where total fat mass decreased by 56 % (Fig. 5D) with reductions in individual adipose tissue deposits of 73 % in SCW and 50 % in eWAT (Fig. 5E). Importantly, liver tissue mass remained largely unchanged, demonstrating tissue specificity and safety. Adiposity index was also significantly reduced by 43 % in *siDPP4-mIL27@LNP-GNc* treated mice, demonstrating considerable improvement to composition of lean muscle mass compared to overall fat mass (Fig. 5F). These results underline the ability of *siDPP4-mIL27@LNP-GNc* to mitigate obesity while preserving healthy organ function.

2.8. siDPP4-mIL27@LNP-GNc reduces macrovesicular lipid droplet deposition, adipocyte size, and activate adaptive thermogenesis in liver and fat tissue

Histological examination was conducted to assess tissue-level changes in liver and adipose tissues following treatment with *siDPP4-mIL27@LNP-GNc* and the corresponding controls. In liver tissue, Oil Red O staining revealed an 18.8 % area reduction of macrovesicular lipid droplets in the *siDPP4-mIL27@LNP-GNc*-treated mice compared to control groups (Fig. 6E). The liver tissues of mice in treatment groups *siDPP4@LNP, mIL27@LNP*, and *siDPP4-mIL27@LNP* also demonstrated reduction in both size and occurrence of macrovesicular lipid droplets, but to a lesser extent compared to *siDPP4-mIL27@LNP-GNc*. While control group livers displayed large lipid droplets typical of steatosis, treatment reduced both the size and number of these droplets, suggesting improved lipid metabolism and reduced fat accumulation directly within the liver tissue and indicating systemic benefits following treatment (Fig. 6 A).

In eWAT, and SCW, H&E staining revealed morphologically smaller adipocytes in all treatment groups compared to controls. The decrease in adipocyte size is indicative of enhanced lipid oxidation and lipolytic activity, as both processes supported by IL-27 activation, PGC-1α, and PPARα signaling. In eWAT the average adipocyte area was significantly

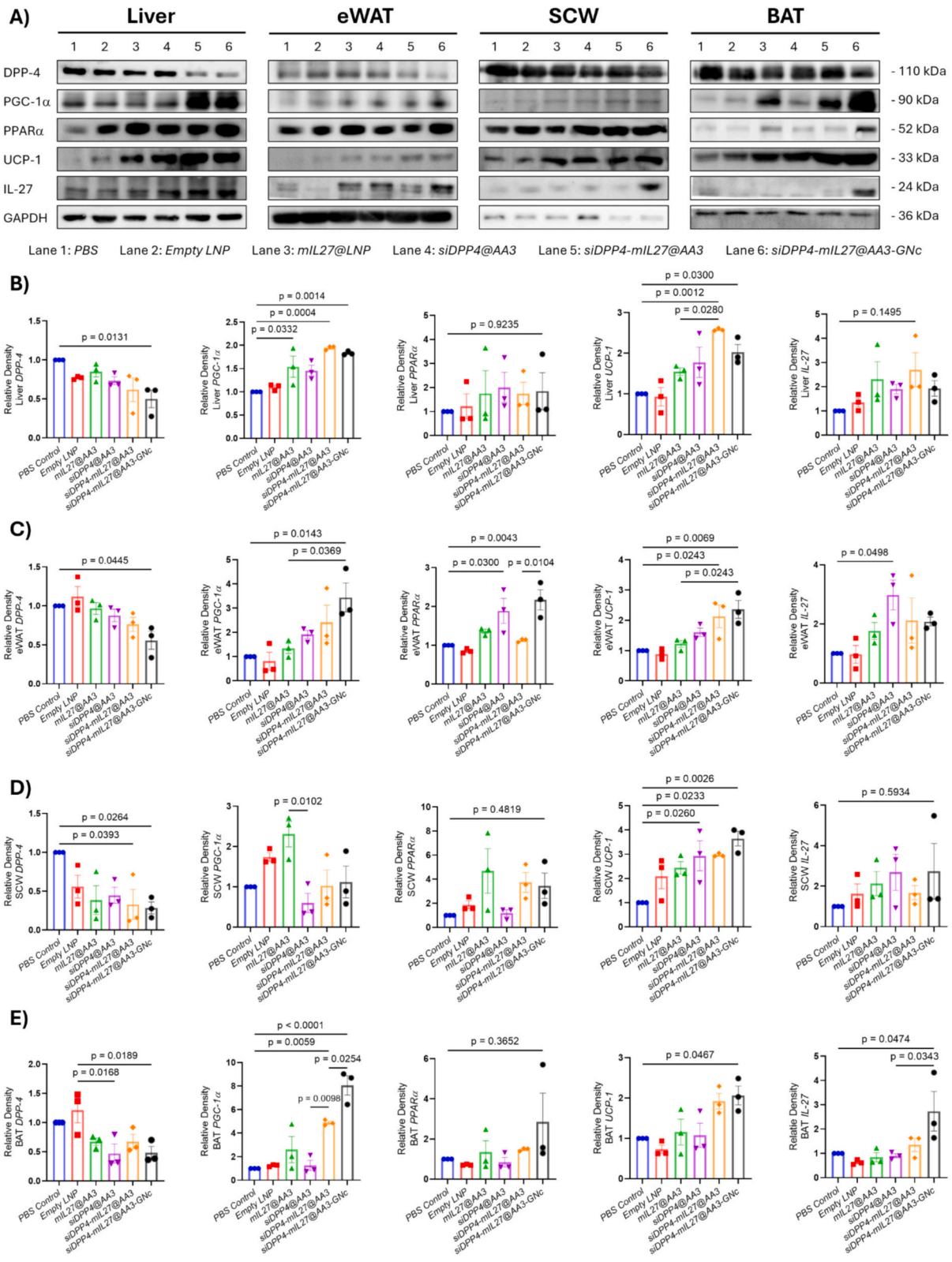

Fig. 4. *siDPP4-mIL27@LNP-GNc* downregulates DPP-4, and upregulates IL-27 expression in hepatocytes, stimulating canonical upregulation of the thermogenic coactivators PGC-1α, PPARα, and UCP-1 in eWAT, SCW, and BAT (A) Immunoblot analysis of liver, eWAT, SCW, and BAT homogenates to investigate DPP-4, PGC-1α, PPARα, UCP-1, IL-27, and GAPDH tissue expression. Treatments are ordered from left to right as *PBS Control, Empty LNP, mIL27@LNP, siDPP4@LNP, siDPP4-mIL27@LNP*, and *siDPP4-mIL27@LNP-GNc.* (B-E) ImageJ quantification of western blot band density for proteins of interest relative to GAPDH in liver, eWAT, SCW, and BAT tissue homogenates ($n = 3$ biological replicates). Results are presented as means ± SEM, and statistical significance was assessed using one-way ANOVA with Tukey test.

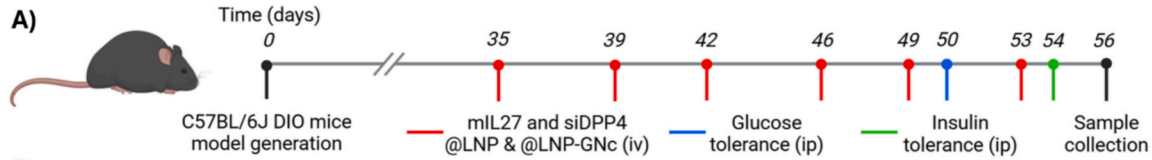

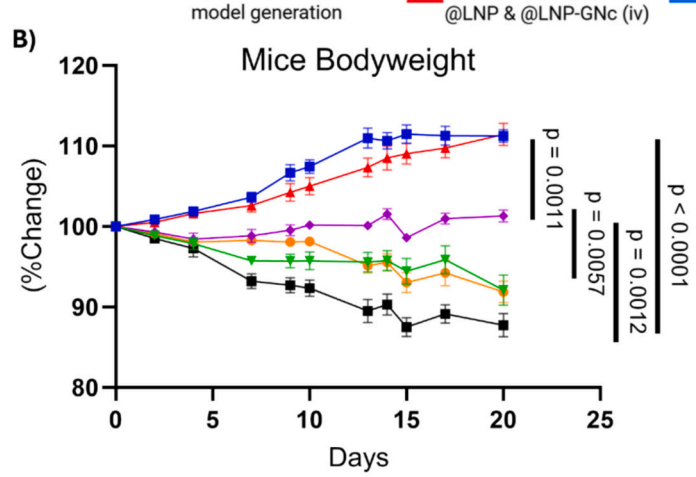

Treatment Group	% Change Bodyweight	% Change from Control
PBS Control	111.3%	0.0%
Empty LNP	111.4%	0.2%
mIL27@LNP	92.1%	-17.2%
siDPP4@LNP	101.3%	-8.9%
siDPP4-mIL27@LNP	91.9%	-17.4%
siDPP4-mIL27@LNP-GNc	87.8%	-21.1%

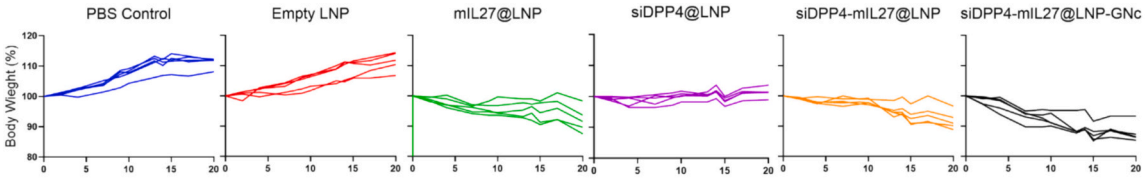

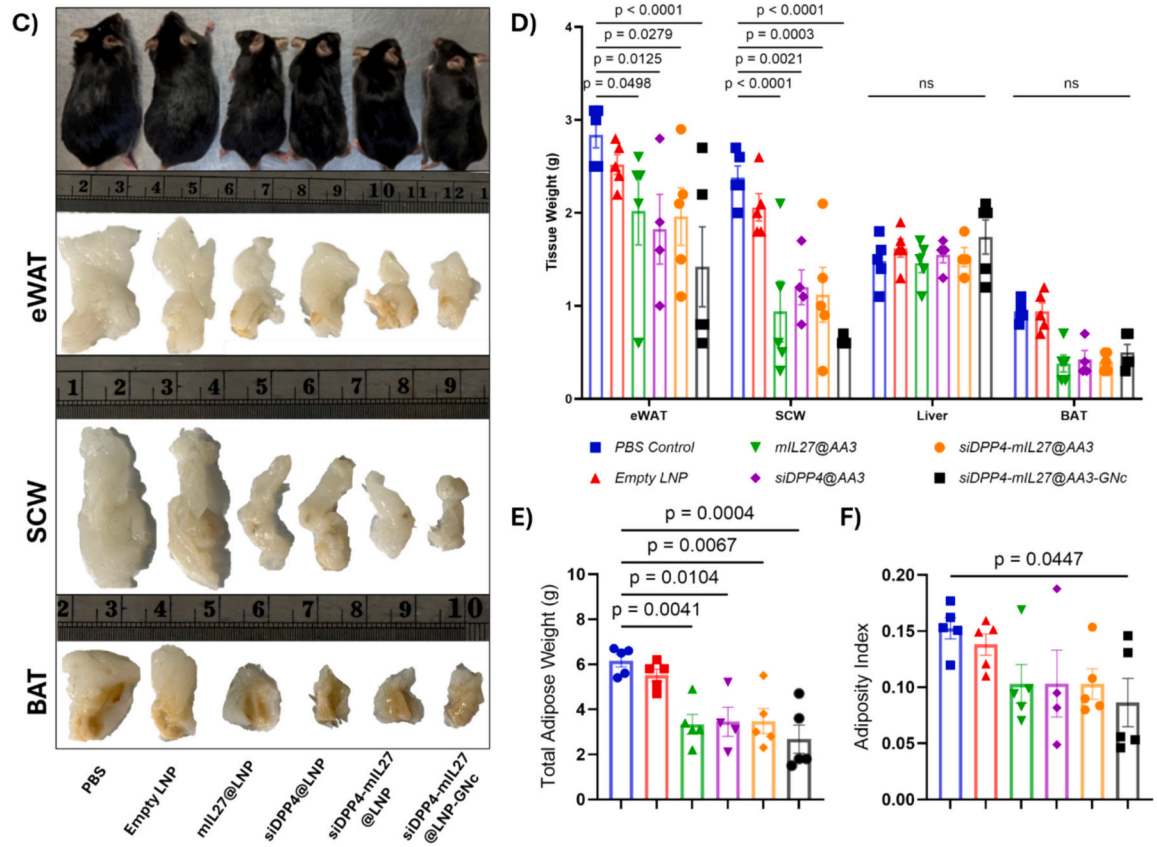

(caption on next page)

Fig. 5. Treatment with *siDPP4-mIL27@LNP-GNc* reduces overall mice bodyweight, and improves insulinotropic activity and glucose homeostasis by silencing hepatic DPP-4 and secreting IL-27 to activate the P38MAPK-PGC-1α signaling pathway. (A) Experimental timeline for dosing with *siDPP4@LNP, mIL27@LNP, siDPP4-mIL27@LNP*, and *siDPP4-mIL27@LNP-GNc*. (B) Average normalized bodyweight reduction of mice over 3 weeks of treatment. Individual mice bodyweight measurements separated according to treatment group over 3 weeks of treatment. ($n = 5$) (C) Representative images of mice, epididymal white adipose (eWAT), subcutaneous inguinal white adipose (SCW), and interscapular brown adipose (BAT) tissues for each treatment group after 3 weeks of treatment. (n = 5) (D) Tissue weights for SCW, eWAT, Liver, and BAT (n = 5). (E) Average total adipose tissue for each treatment group (n = 5). (F) Mice adiposity index of total fat mass relative to total bodyweights to indicate degree of obesity is significantly reduced in *siDPP4-mIL27@LNP-GNc* treatment group (n = 5). Results for Total adipose weight (E) and Adiposity index (F) are presented as mean ± SEM, and statistical significance was assessed using one-way ANOVA with Tukey test (ns > 0.05). Results for Mice Bodyweight (B) and Tissue weight (D) are presented as mean ± SEM, and statistical significance was assessed using two-way ANOVA with Tukey test (ns > 0.05). (For interpretation of the references to colour in this figure legend, the reader is referred to the web version of this article.)

reduced in the targeting combinatorial group, *siDPP4-mIL27@LNP-GNc* (1236 μm^2), compared to both the non-targeting combinatorial group, *siDPP4-mIL7@LNP* (1911 μm^2), the less effective individual RNA groups, *siDPP4@LNP* (3327 μm^2) and *mIL27@LNP* (3617 μm^2), and the control groups *Empty LNP* (3943 μm^2) and *PBS Control* (4259 μm^2) (Fig. 6I). SCW demonstrated similar trends in reduced average adipocyte area with *siDPP4-mIL27@LNP-GNc* (851 μm^2) generating the smallest adipocytes, followed by *siDPP4-mIL7@LNP* (2212 μm^2), *siDPP4@LNP* (3018 μm^2), *mIL27@LNP* (3631 μm^2), and the control groups *Empty LNP* (3901 μm^2) and *PBS Control* (3854 μm^2) (Fig. 6 J). In eWAT, SCW, and BAT, treatment with *siDPP4-mIL27@LNP-GNc* led to increased UCP-1 expression, indicating adipocyte browning, lipid mobilization, and enhanced thermogenic activity (Fig. 6D). All adipose tissues from treated mice displayed greater UCP-1 expression, suggesting increased mitochondrial activity and providing molecular support for adaptive thermogenesis, the key therapeutic process stimulating increased energy expenditure and mass reduction directly within adipocytes. Treatment with *siDPP4-mIL27@LNP-GNc* resulted in the greatest upregulation of UCP-1 as determined by IHC staining, with percent area increases of 20.6 %, 12.3 %, and 38.4 % in eWAT, SCW, and BAT, respectively, compared to *PBS Control* (Fig. 6F–H). These histopathological results demonstrate that *siDPP4-mIL27@LNP-GNc* treatment effectively reduces lipid accumulation in the liver and adipocyte size in adipose tissues, while simultaneously activating adipocyte differentiation and thermogenesis directly within adipocytes.

2.9. siDPP4-mIL27@LNP-GNc enhances glucose tolerance and insulin sensitivity

To further investigate metabolic improvements after treatment, we assessed glucose tolerance and insulin sensitivity. Glucose tolerance testing (1 g/kg glucose) revealed enhanced glucose tolerance, characterized by lower peak postprandial blood glucose levels and reduction in area under the curve following treatment with *siDPP4-mIL27@LNP-GNc* (26 %), *siDPP4-mIL27@LNP* (24 %), *siDPP4@LNP* (15 %), and *mIL27@LNP* (17 %), indicative of enhanced insulinotropic activity (Fig. 7B). Complementary insulin tolerance testing (0.75 U/kg insulin) corroborated these findings, with significant reduction in changes of postprandial blood glucose demonstrated by reduction in area under the curve following treatment with *siDPP4-mIL27@LNP-GNc* (20 %), *siDPP4-mIL27@LNP* (16 %), *siDPP4@LNP* (7 %), and *mIL27@LNP* (8 %), indicative of improved insulin resistance (Fig. 7C). Poor performing groups in these assessments demonstrated exaggerated hypoglycemic responses and delayed recovery, reflecting impaired endogenous insulin function.

Serum analysis further supported these results, showing an 81 % decrease in basal insulin levels in the *siDPP4-mIL27@LNP-GNc* group, followed by *siDPP4-mIL27@LNP* (71 %), *siDPP4@LNP* (49 %), and *mIL27@LNP* (49 %) (Fig. 7E). These findings demonstrate that targeted dual *siDPP4-mIL27@LNP-GNc* therapy effectively restores metabolic homeostasis by improving glycolytic activity and restoring insulin sensitivity.

2.10. siDPP4-mIL27@LNP-GNc modulates adipokine concentration in serum

Given the interplay of adipokines in obesity and metabolism, we evaluated serum levels of adiponectin and leptin. Adiponectin, an adipocyte secreted hormone inversely correlated with obesity, enhances insulin sensitivity due to activation of activated protein kinase pathway (AMPK) in muscle and liver tissues to promote glucose uptake, fatty acid oxidation, and glycolysis. Adiponectin also suppresses pro-inflammatory pathways including NF-kB signaling to reduce systemic inflammation, while supporting adipocyte tissue remodeling by stimulating white-to-brown adipocyte differentiation and adaptive thermogenesis. Serum adiponectin concentrations were significantly increased by 86 % in the *siDPP4-mIL27@LNP-GNc* treatment, while nonsignificant increases of 50 %, 36 %, and 32 % were observed in the *siDPP4-mIL27@LNP, mIL27@LNP*, and *siDPP4@LNP* treatments, respectively (Fig. 7F).

Conversely, serum leptin levels decreased across all treatment groups, with the greatest reduction observed in the *siDPP4-mIL27@LNP-GNc* group (54 %), followed by *siDPP4-mIL27@LNP* (47 %), *siDPP4@LNP*(46 %), and *mIL27@LNP* (37 %) (Fig. 7G). Leptin, another adipocyte-secreted hormone, is secreted proportionally to adipose tissue mass and regulates appetite and energy homeostasis via hypothalamic signaling. However, obesity-induced hyperleptinemia leads to leptin resistance and receptor desensitization, impairing its metabolic functions. Reduction of leptin concentrations can resensitize pathophysiological responses for appetite suppression, enhance thermogenesis, and promote weight.

2.11. siDPP4-mIL27@LNP-GNc modulates secondary serum metabolic biomarkers

Beyond incretin system and adipokine related functions, quantification of secondary serum biomarkers including free fatty acids, cholesterol, and triglycerides, provided additional insights into indirect improvements to metabolic health after treatment with *siDPP4-mIL27@LNP-GNc*. Measurement of serum free fatty acids (FFA) demonstrated non-significant decreases across treatment groups, likely due to variability in non-treated controls (Fig. 7I). FFA reduction is linked to enhanced insulin sensitivity, suppressing lipolysis via hormone-sensitive lipase (HSL) and increased fatty acid utilization through AMPK activation and P38MAPK-PGC-1α signaling, promoting oxidation and thermogenesis. Significant reductions in total serum cholesterol were observed across all treatment groups, with the *siDPP4-mIL27@LNP-GNc* group achieving the greatest decrease of 49 %, followed by *siDPP4-mIL27@LNP* (40 %), *mIL27@LNP* (37 %), and *siDPP4@LNP* (30 %) (Fig. 7 J). Concurrently, serum triglycerides were also significantly reduced by 51 % in the *siDPP4-mIL27@LNP-GNc* group and 42 % in the *siDPP4-mIL27@LNP* group (Fig. 7 K). These reductions indicate improved lipid metabolism, helping to counteract obesity-associated dyslipidemia, characterized by elevated VLDL and LDL, reduced HDL, excessive triglyceride production from dysregulated lipolysis, and impaired triglyceride clearance due to downregulated lipoprotein lipase activity. Treatments that lower serum cholesterol and rebalance lipoprotein levels reduce cardiovascular and atherogenic risk. Additionally, activation of adipose tissue differentiation and PPAR

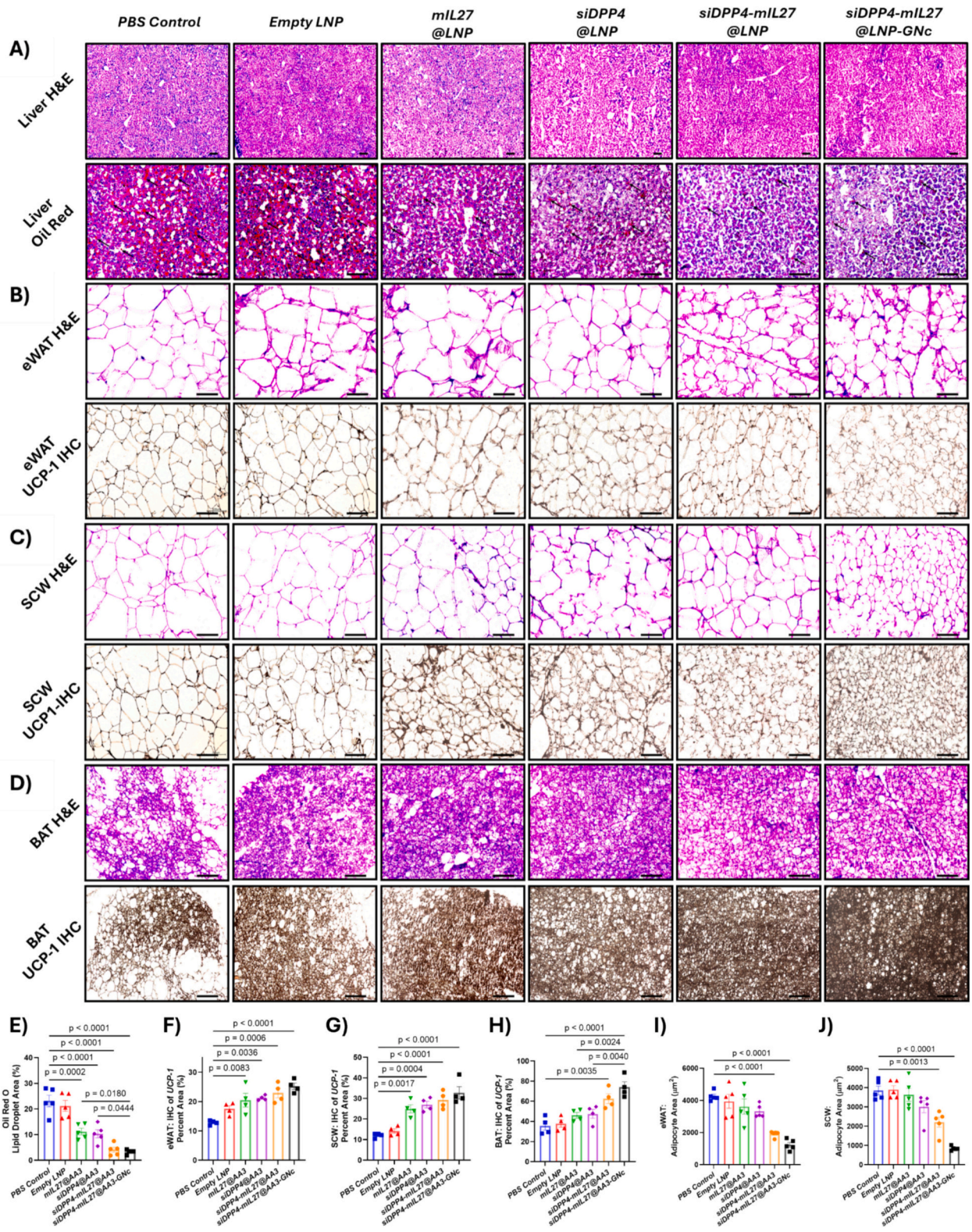

Fig. 6. *siDPP4-mIL27@LNP-GNc* treatment reduces macrovesicular lipid droplet accumulation within liver tissue, and reduces adipocyte size and morphology in eWAT, SCW, and BAT. *siDPP4-mIL27@LNP-GNc* treatment silences hepatic DPP-4 and secretes hepatic IL-27 to activate the P38MAPK-PGC-1α signaling pathway, and stimulate adaptive thermogenesis via upregulation of UCP-1. (A) Representative images of liver tissue sections stained with Hematoxylin Eosin (H&E, Top), and Oil Red O (Bottom, Lipid droplets are red, examples indicated by arrows). (B–D) Representative images of eWAT (B), SCW (C), and BAT (D) sections stained with H&E (Top), and Immunohistochemistry staining of UCP-1 (Bottom). Scale bars 100 μm. (E) Quantification of lipid droplet percent area in liver tissue measured by Oil Red O staining after 3 weeks of treatment ($n = 5$). (F–H) Percent area quantification of IHC staining of UCP-1 in eWAT (F), SCW (G), and BAT (H) tissues after 3 weeks of treatment ($n = 4$). (I-J) Quantification of mean adipocyte area for eWAT (I) and SCW (J) after 3 weeks of treatment (n = 5). Results are presented as mean ± SEM, and statistical significance was assessed using one-way ANOVA with Tukey test.

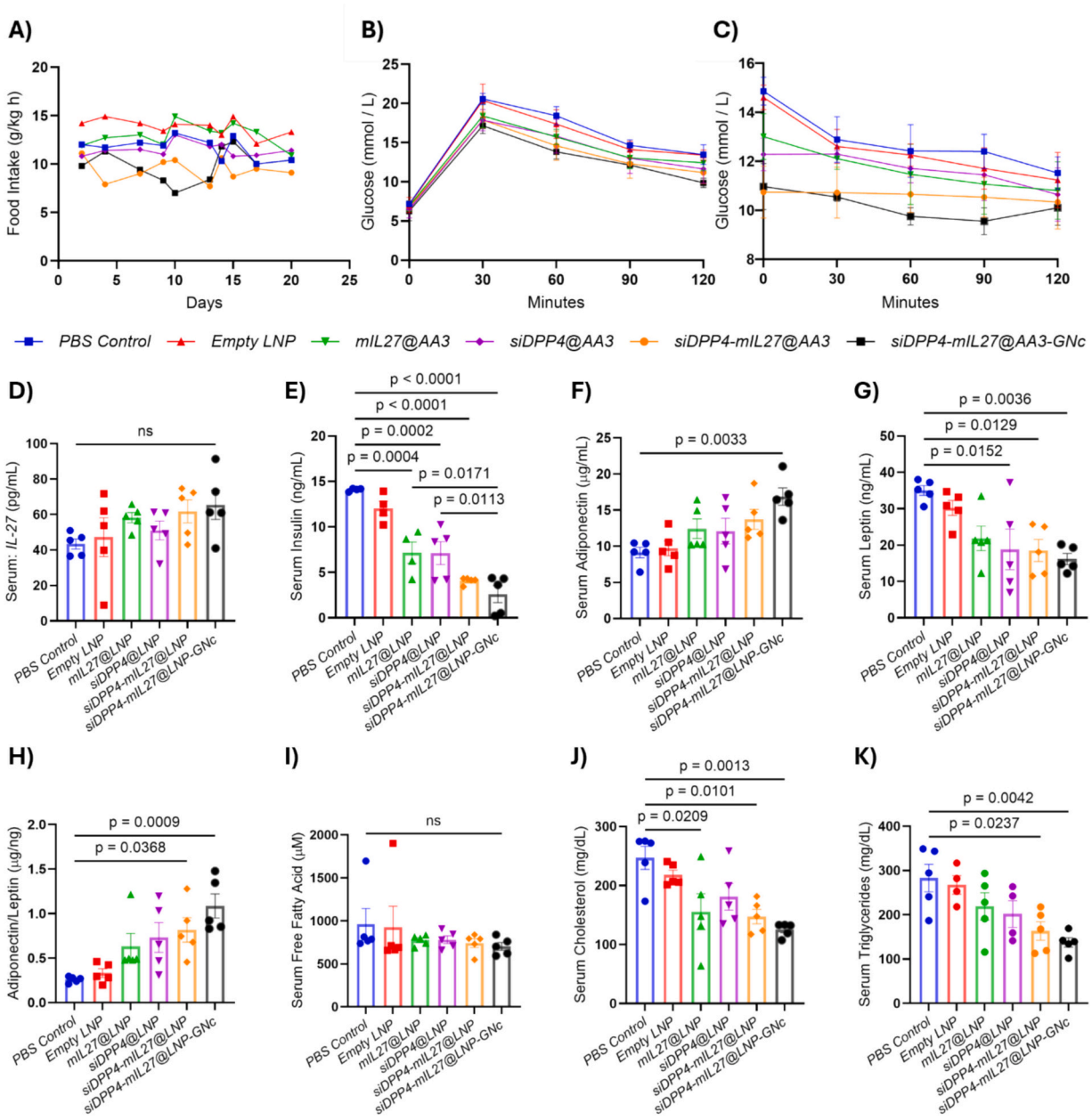

Fig. 7. *siDPP4-mIL27@LNP-GNc* treatment reduces overall mass of individual eWAT, SCW, and BAT tissue deposits via increases in insulinotropic activity, and activation of adaptive thermogenesis. Combinatorial RNA-based treatment results in improvements to serum concentrations of key incretin system related adipokines, and metabolic health biomarkers. (A) Food intake for mice during 3 weeks of treatment. (B) Glucose tolerance testing of fasted blood glucose response after intraperitoneal (i.p.) administration of glucose ($n = 5$). (C) Insulin tolerance testing of fasted blood glucose response after i.p. administration of insulin (n = 5). (*E*-L) Serum concentration of key adipokine and metabolic health biomarkers related to obesity (n = 5). Results are presented as mean ± SEM, and statistical significance was assessed using one-way ANOVA with Tukey test (ns > 0.05).

receptor stimulation enhances fatty acid oxidation, limiting triglyceride synthesis and reducing circulating levels, ultimately supporting improved metabolic health. These reductions, coupled with nonsignificant decreases in free fatty acids, align with enhanced hepatic fatty acid utilization and systemic lipid clearance, reinforcing the therapeutic promise of targeted LNPs.

2.12. *In vivo safety evaluation*

Histological analysis of major organs from DIO mice treated with *@LNP* and *@LNP-GNc* containing *siDPP-4* and *mIL-27* showed no significant changes in organ size, morphology, or signs of injury in liver, heart, kidney, and lung tissues (Fig. 8A). In vivo safety evaluation revealed improvements to blood biochemical markers, including serum triglycerides, cholesterol, and free fatty acids, compared to control groups (Fig. 8B-E). Additionally, lipid droplet deposition in liver tissue was markedly reduced in *@LNP* and *@LNP-GNc* treatment groups, while PBS and empty LNP controls showed large macrovesicular lipid droplets (Fig. 6 A). These findings, along with the absence of injury in tissue analysis, indicate that *@LNP* and *@LNP-GNc* are safe at the tested dosage.

3. Discussion

Obesity, a complex metabolic disorder characterized by excessive adiposity and disrupted metabolic homeostasis, remains a significant

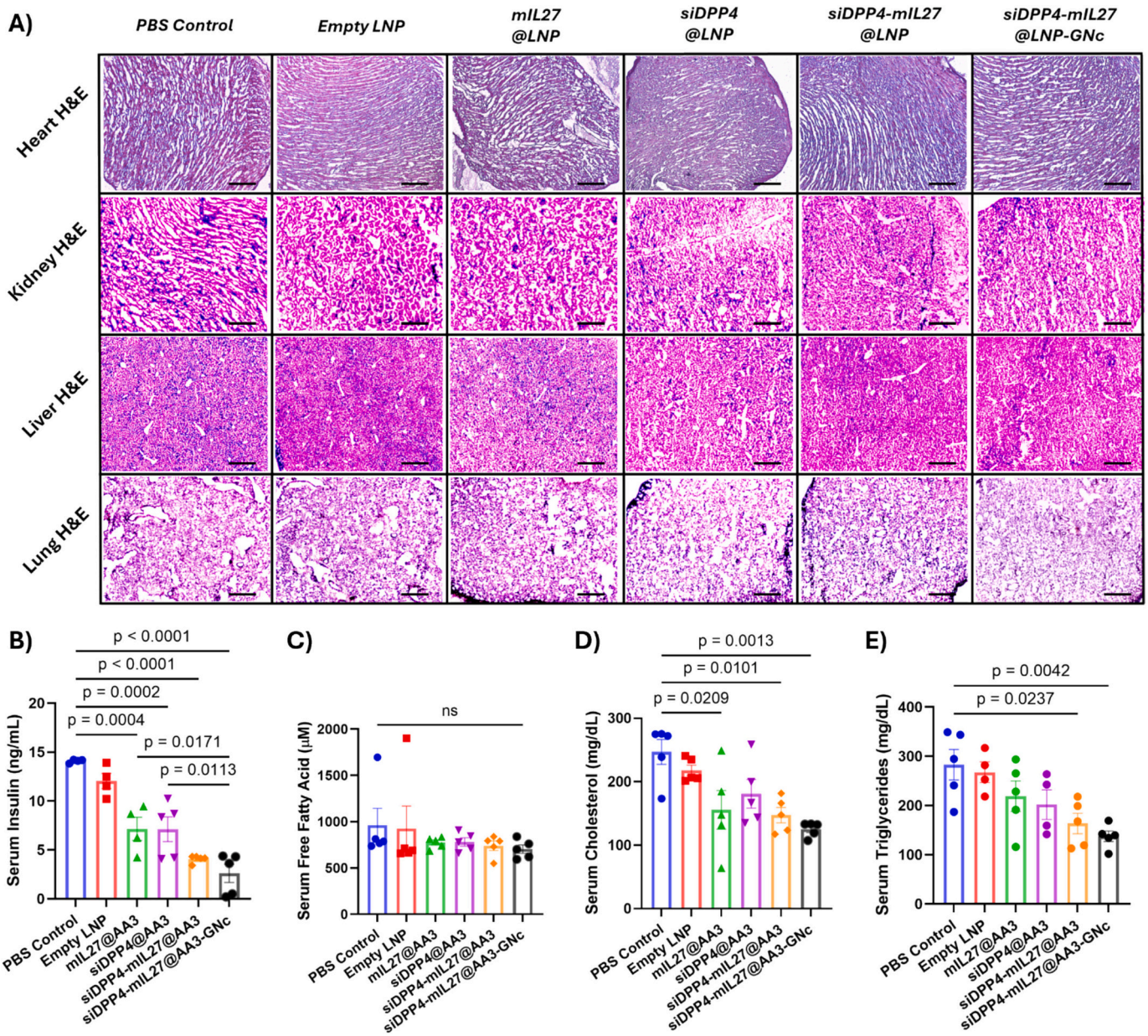

Fig. 8. In vivo safety evaluation. (A) Histopathological analysis of heart, kidney, liver, and lung of DIO mice model following treatment with *PBS, Empty LNP, siDPP4@LNP, mIL27@LNP, siDPP4-mIL27@LNP*, and *siDPP4-mIL27@LNP-GNc*. H&E staining of heart, kidney, liver, and lung do not show any signs of observable injury within the different treatment groups. Scale bars 500 μm. (B-E) Biochemical blood biomarker indicators for overall metabolic health. Improvements to serum insulin (B), free fatty acid (C), cholesterol (D), and triglycerides (E) values after treatment *with siDDP-mIL27@LNP-GNc* indicate positive metabolic health effects and demonstrate robust safety profiles at the examined dosage ($n = 5$). Results are presented as mean ± SEM, and statistical significance was assessed using one-way ANOVA with Tukey test.

health challenge globally. This condition is closely linked to a range of comorbidities, including type 2 diabetes, cardiovascular disease, and certain cancers, leading to increased morbidity and mortality [1–5]. Although current pharmacological therapies, such as GLP-1 receptor agonists (e.g., Ozempic® and Mounjaro®), have shown promise in weight reduction by modulating the incretin system, they are limited by suboptimal responses in a subset of patients and often result in nonspecific weight loss, including the undesirable loss of lean muscle mass [7,9,16,17]. Moreover, these therapies may be associated with limitations to therapeutic potential due to receptor targeting exclusively within the incretin system, and not adequately addressing the multifaceted mechanisms underlying obesity. Therefore, there is an urgent need for alternative and complementary strategies that can address both the reduction of energy intake and the enhancement of energy expenditure in a more targeted and comprehensive manner.

The co-delivery of siRNA and mRNA represents a robust therapeutic approach capable of modulating multiple aspects of metabolic regulation. In this study, *siDPP-4* was selected to specifically target dipeptidyl peptidase-4, a serine protease that inhibits the incretin hormones, GLP-1 and GIP [31,32,33]. The subsequent prolonged activation of GLP-1 and GIP receptors enhances insulinotropic effects, improves insulin sensitivity, and activates cAMP signaling cascade to promote pancreatic β-cell function and facilitate enhanced glycolytic activity, thereby reducing energy intake by improving glucose utilization [8,9,11,38]. Simultaneously, *mIL-27* encodes interleukin-27, a hepatocyte secreted cytokine that activates the P38MAPK-PGC-1α signaling pathway to stimulate increased energy expenditure. IL-27-mediated coactivation of thermogenic regulators PGC-1α, PPARα, and UCP-1 promotes oxidative

metabolism, mitochondrial biogenesis, adipocyte differentiation, and adaptive thermogenesis [23,24,35,39]. Both *mIL-27@LNP* and *siDPP-4@LNP* LNPs were successfully prepared resulting in monodisperse, ~88 nm particles, with encapsulation efficiencies over 95 %. Experimental validation revealed that *siDPP-4* delivery achieved a 21 % reduction in DPP-4 mRNA expression in liver tissue after 6 biweekly treatments with *siDPP4@LNP* in a DIO murine model. Simultaneously, treatment with *mIL-27@LNP* in a DIO murine model achieved a 1.9-fold increase in hepatic IL-27 RNA expression, correlating with elevated circulating IL-27 concentrations and enhanced thermogenic signaling in peripheral adipose tissues. Functional assays demonstrated that *siDPP4@LNP* and *mIL27@LNP* treatments both decreased serum insulin levels by 49 %. *mIL27@LNP* was shown to upregulated thermogenic markers PGC-1α, PPARα, and UCP-1 by 20.2-, 10.8-, and 5.5-fold respectively, in eWAT. *siDPP4@LNP* demonstrated similar results in eWAT, upregulating PGC-1α, PPARα, and UCP-1 by 23.7-, 5.3-, and 5.4-fold respectively. The ability of these RNAs to independently reduce body weight, 8.9 % for *siDPP4@LNP* and 17.2 % for *mIL-27@LNP,* underscores their individual therapeutic potential and sets the stage for their combination in a single platform.

Combining *siDPP-4* and *mIL-27* within the same *@LNP* formulation yielded pronounced synergistic effects in our DIO murine model, significantly outperforming either individual RNA therapy. Encapsulation of both *siDPP4* and *mIL27* into a co-delivery LNP, *siDDP4-mIL27@LNP*, had minimal effect on physical characteristics, resulting in particle sizes of ~97 nm, and encapsulation efficiency above 95 %. Subsequent administration of *siDPP4-mIL27@LNP* into our DIO murine model achieved a 34 % reduction in DPP-4 mRNA expression in liver tissue, and 2.36- fold increase of hepatic IL-27 expression after 6 biweekly treatments. Additionally, *siDPP4-mIL27@LNP* decreased serum insulin levels by 71 %, while upregulating thermogenic markers PGC-1α, PPARα, and UCP-1 by 30.9-, 11.1-, and 6.8-fold respectively, in eWAT. The upregulation of thermogenic biomarkers was also observed systemically in other adipose tissue deposits with increases of PGC-1α, PPARα, and UCP-1 by 48.8-, 44.1-, and 173-fold respectively in SCW, and 3.0-, 40.5-, and 3.4-fold respectively in BAT. The synergistic improvement in metabolic function and activation of thermogenic biomarkers had an additive effect, resulting in a 17.4 % reduction in body weight after three weeks of treatment, accompanied by a 43 % reduction in fat mass and a 32 % improvement in adiposity index. The synergistic benefits of the combinatorial therapeutic are likely due to complementary mechanisms, induced by *siDPP-4* to enhance glucose homeostasis by promoting prolonged incretin receptor stimulation and, *mIL-27* for the activation of adaptive thermogenesis and browning of white adipose tissue deposits.

The liver, as a metabolic nexus, was strategically chosen for targeted RNA delivery to address obesity's multifaceted pathophysiology, due to its pivotal roles in glucose regulation, lipid metabolism, and systemic energy balance [19]. Hepatocytes play a central role in integrating metabolic and inflammatory signals, making them ideal targets for RNA-based therapeutics. Targeting DPP-4 and IL-27 expression in hepatocytes serves to reduce both local liver inflammation and systemic metabolic dysregulation by activating insulinotropic and thermogenic pathways. The GalNAc-modified *@LNP-GNc* were engineered for specific uptake by Asialoglycoprotein receptors (ASGPR) on hepatocytes, achieving unparalleled targeting efficiency [20–22]. In vivo imaging studies using *mLuc@LNP-GNc* revealed an 48-fold increase in average radiance localized to the liver after 24 h compared to the non-targeting control *mLuc@LNP*, with negligible accumulation in non-hepatic tissues. Functionally, this enhanced targeting translated into significant improvements in RNA activity, where treatment with *siDPP4-mIL27@LNP-GNc* reduced hepatic DPP-4-RNA expression by 60 %, and amplified *mIL-27* expression by 2.79- fold. The increased translational effects from the targeted *@LNP-GNc* were able to further decrease serum insulin levels by 81 %, and improved insulinotropic activity by reducing glucose area under the curve values by 26 % and 20 % in glucose and insulin tolerance tests, respectively. Treatment with *siDPP4-mIL27@LNP-GNc* generated the greatest systemic response in the upregulation of thermogenic biomarkers, PGC-1α, PPARα, and UCP-1, across all evaluated adipose tissues, resulting in 44.5-, 27.1-, and 7.2-fold increases in eWAT, 270-, 529-, and 640-fold increases in SCW, and 17.1-, 195-, and 20.1-fold increases in BAT. Collectively, the systemic activation of insulinotropic and thermogenic activity from the targeted codelivery of *siDPP4-mIL27@LNP-GNc* stimulated a significant 21.1 % reduction of bodyweight in our DIO murine model, as well as a 56 % reduction in total fat mass, and 43 % improvement to adiposity index. These improvements in liver targeting and biodistribution were not only critical for achieving the observed therapeutic outcomes, but also reduced systemic exposure, mitigating potential side effects.

Beyond the primary outcomes of weight loss and adiposity reduction for our targeted dual-RNA approach, administration of *siDPP4-mIL27@LNP-GNc* also improved a range of secondary metabolic markers in a DIO murine model, underscoring its broader efficacy in combating obesity-related pathophysiology. Blood biochemistry revealed significant reductions in serum cholesterol (49 %) and triglycerides (51 %), along with a 26 % reduction of free fatty acids, which could not be determined as significant due to large background variability in the control samples. The reduction of serum biochemical markers reflects broad improvements in metabolic function stimulated by lipolysis, fatty acid metabolism and lipid utilization. Similarly, an 86 % increase in adiponectin and a 54 % decrease in leptin following treatment with *siDPP4-mIL27@LNP-GNc* suggest improved adipose tissue function and restored metabolic homeostasis through enhanced systemic regulation and resensitization of insulin and leptin receptors [40]. Histological analyses of liver tissue after *siDPP4-mIL27@LNP-GNc* treatment demonstrated a marked reduction of 19.8 % in macrovesicular lipid droplet deposition, and improvement to steatosis as determined by Oil Red O staining. In adipose tissue, H&E staining revealed significantly reduced adipocyte size with decreases to average adipose area of 3023 μm^2 and 3003 μm^2 in eWAT and SCW, respectively. UCP-1 density, as determined by immunohistochemical staining, increased by 12.3 % (eWAT), 20.6 % (SCW), and 38.4 % (BAT), consistent with adipose differentiation toward brown/beige adipocyte phenotypes and enhanced thermogenic activity due to IL-27 activation of the P38MAPK-PGC-1α signaling pathway. These cellular changes were largely reflected in the comprehensive metabolic improvements to the secondary and indirect biomarkers that are dysregulated in obesity. Together, these results demonstrate that the *siDPP4-mIL27@LNP-GNc* therapeutic platform exerts pleiotropic effects, improving metabolic health far beyond weight loss alone.

While qPCR analyses exhibited comparable DPP-4 mRNA knockdown in both siDPP4@LNP and siDPP4-mIL27@LNP groups, Western blot analysis revealed a notable discrepancy in protein-level expression between these groups. However, only the targeted formulation, siDPP4-mIL27@LNP-GNc, achieved statistically significant DPP-4 protein knockdown relative to controls. This highlights the importance of GalNAc-mediated hepatocyte targeting and suggests that additional factors such as improved delivery efficiency, increased liver accumulation, or increased siRNA dosage may be critical contributors to effective protein-level silencing. The temporal lag between mRNA degradation and protein turnover, especially for a relatively stable protein like DPP-4, may further explain the observed discrepancy. These results underscore the need for further optimization of therapeutic dosing and scheduling, and raise the possibility of synergistic enhancement of siRNA efficacy when co-delivered with immunomodulatory mRNAs. Future studies will be directed at dissecting these synergistic effects and improving translational control through combined RNA modalities.

The findings of this study underscore the potential of a dual RNA-based therapeutic strategy targeting obesity and metabolic dysfunction, while highlighting several areas for continued refinement. For future work, optimizing the dosing concentrations and co-delivery ratios of *mIL-27* and *siDPP4* will be crucial for maximizing therapeutic efficacy

and safety. Fine-tuning these parameters could further enhance the synergistic effects of *mIL-27* and *siDPP4* delivery. Additionally, incorporating GLP-1 receptor agonists or other benchmark therapies in future experiments will provide valuable comparisons, strengthening the translational potential of this method. Expanding research to include more complex animal models, such as diet-induced obese nonhuman primates, will be crucial for evaluating the therapy's effectiveness in settings that better mimic human obesity and its comorbidities. This approach also offers opportunities to explore long-term safety, therapeutic durability, and potential cardiovascular benefits, including improved lipid profiles, reduced systemic inflammation, and enhanced endothelial function. Expanding the scope of research to encompass nonalcoholic fatty liver disease (NAFLD) and nonalcoholic steatohepatitis (NASH) would provide valuable insights into the therapy's capacity to ameliorate liver-specific dysfunction. Given the strong correlation between obesity, metabolic disorders, and hepatic steatosis, this dual RNA-based therapy could serve as a complementary strategy to mitigate steatosis, reduce lipid accumulation, and improve overall liver function. Future studies in NAFLD and NASH models should assess its impact on hepatic triglyceride deposition, fibrosis progression, and inflammatory pathways, while collaborative efforts on NASH reversal could further validate its role in mitigating liver pathology. This versatile framework not only enhances metabolic health but also establishes a complementary foundation for tackling the intertwined challenges of obesity and liver disease.

In conclusion, we have demonstrated a promising dual RNA-based, targeted therapeutic approach for the treatment of obesity and metabolic dysfunction. By combining the hepatocyte-targeted delivery of *mIL-27* and *siDPP-4*, we successfully modulated both the incretin system and adipocyte thermogenesis, leading to a significant 21.1 % weight loss, and 56 % reduction in total fat mass in a DIO murine model. This strategy represents a promising alternative to current pharmacotherapies, addressing key limitations in obesity treatment by targeting multiple pathways involved in regulating the incretin system and adipocyte thermogenesis, effectively rebalancing both energy intake and expenditure. Future advancements in delivery optimization and translational studies will be essential to further unlock its full clinical potential. With further refinement and validation, this dual combinatorial RNA strategy has the potential to establish a new paradigm in obesity treatment, offering significant improvements to patient outcomes while mitigating risks for associated comorbidities including cardiovascular disease and type 2 diabetes.

4. Materials and methods

4.1. Materials

1,2-distearoyl-sn-glycero-3-phosphocholine (DSPC), cholesterol, and 1,2-dimyristoyl-rac-glycero-3-methoxypolyethylene glycol-2000 (DMG-PEG2000) were purchased from Avanti Polar lipids. Sodium acetate buffers, Candida Antarctica Lipase B Immobilized (CALB), Linoleic acid, 1,4-Bis(2-hydroxythyl)piperazine, Cell Counting Kit-8 (CCK-8), anhydrous Magnesium sulfate, Sodium bicarbonate, Tetrahydrofuran, Amicon Ultracentrifuge Filters (MWCO 50 kDa), Dialysis kits (MWCO 3.5 kDa), RIPA 10× Lysis Buffer, ReadyShield Phosphatase Inhibitor Cocktail, and Protease Inhibitor Cocktail were all available from Sigma-Aldrich. Mouse Adiponectin ELISA Kit, Mouse Leptin ELISA kit, Rat/Mouse Insulin ELISA kit, Free Fatty Acid Assay kit, Cholesterol Quantification Assay Kit were purchased from Sigma-Aldrich. Mouse IL-27 ELISA kit, and 1,1'-Dioctadecyl-3,3,3′,3'-Tetramethylindotricarbocyanine Iodide (DiR) dye was purchased from ThermoFisher. Triglyceride Colorimetric assay kit was available from Cayman Chemical. One Touch Ultra 2 glucose meter, and strips were purchased from Amazon. SuperScript IV Reverse Transcriptase, PowerUp SYBR Green Master mix, DH5 Alpha competent cells, and PageRuler Prestained Protein Ladder were purchased from ThermoFisher. Oil Red O Staining Kit was purchased from VitroVivo Biotech. AmpliScribe T7-Flash Transcription Kit was purchased from LGC Biosearch Technologies. 1 kb Plus DNA Ladder, NEBuilder HiFi DNA Assembly master mix, and *Bsa*I HFv2 were purchased from New England BioLabs. CleanCap Reagent AG was purchased from TriLink. Y-UTP was purchased from APExBio. QIAquick PCR Purification System was purchased through Qiagen. RNA Clean & Concentrator and Direct-Zol RNA miniprep kit were purchased from Zymo. eGFP mRNA (N1y) and FLuc (N1y) mRNA were purchased from GenScript. All the cell culture reagents such as Dulbecco's Modified Eagle Medium (DMEM, Fetal Bovine Serum (FBS), 0.25 % Trypsin-EDTA (1×) and Penicillin-Streptomycin, etc. were obtained from Gibco (Paisley, UK). D-Luciferin potassium salt was obtained from PerkinElmer. *siDPP-4* siRNA and primers were purchased from IDT, and sequence information is provided in supplementary table 1. High-Fat Diet (60 kcal from fat) Was purchased from Teklad. Rabbit specific HRP/DAB IHC Detection kit (ab64261), H&E Staining Kit (ab245880), anti-PGC-1 alpha+beta antibody (ab72230), anti-GAPDH antibody (ab313650), anti-UCP-1 antibody (ab209483), anti-PPAR alpha + PPAR beta/delta antibody (ab178865), Goat anti-rabbit IgG (H&L) HRP (ab205718) were purchased from Abcam. Mouse DPPIV/CD26 antibody (AF954), Mouse IL-27 p28/IL-30 antibody (AF1834), and Chicken anti-goat IgG HRP (HAF019) were purchased from R&D Systems. All the other general chemicals and reagents were obtained from Sigma-Aldrich and VWR (Radnor, PA, USA).

4.2. In vitro transcription (IVT) of IL-27 mRNA

The sequences for in vitro transcription of mRNA, including T7 promoter, 5- UTR, IL-27 coding sequence, 3' UTR, and poly(A) (Supplementary table 1) were cloned into pVAX1 vector using NEBuilder® HiFi DNA Assembly Cloning Kit. The mixture was then transformed into DH5a Competent Cells (ThermoFisher) by chemical transformation and the synthesized plasmid was confirmed by Sanger Sequencing. Then, a linearized DNA template, including T7 promoter, 5' UTR, IL-27 coding sequence, 3' UTR, and poly(A) was achieved by *Bsa*I digestion. The DNA templates were purified by QIAquick Gel Extraction Kit (Qiagen) and confirmed by 1 % agarose gel electrophoresis. All mRNAs were synthesized by in vitro transcription with CleanCap (Trilink) and 100 % pseudouridine-5′-triphosphate (APEx-BIO) using AmpliScribe T7-Flash Transcription Kit (LGC Biosearch Technologies) following the manufacturer's instructions. Subsequently, mRNA was purified by RNA Clean & Concentrator (Zymo). The synthesized mRNAs were examined by 1 % agarose gel electrophoresis, and the concentration was measured using a NanoDrop Spectrophotometer (ThermoFisher) prior to storage at —80C for future use.

4.3. Synthesis and characterization of AA3-Dlin and DMG-PEG-GalNAc

AA3-Dlin: The ionizable lipid AA3-Dlin was synthesized following a previously described procedure [37]. In brief, amino alcohol (2.87 mmol) was dissolved in 5 mL of tetrahydrofuran and mixed with lipid acid at a molar ratio of 1: 2. The resulting mixture was catalyzed by CALB and reacted at 60 °C for 72 h under a nitrogen atmosphere. Afterward, the CALB was removed via centrifugation, and the excess lipid acid in the supernatant was neutralized with a saturated NaHCO3 solution. The mixture was extracted by ethyl acetate and dried with anhydrous MgSO4 to yield a lipid ethyl acetate solution. The lipid solution was then concentrated using a rotary evaporator and dried under vacuum for subsequent use. ^{1}H NMR (400 MHz, Chloroform-*d*): δ 5.45–5.23 (m, 8H), 4.19 (t, J = 5.9 Hz, 4H), 2.79–2.71 (m, 4H), 2.69–2.46 (m, 12H), 2.28 (t, J = 7.5 Hz, 4H), 2.03 (q, J = 6.9 Hz, 8H), 1.59 (t, J = 7.4 Hz, 4H), 1.37–1.22 (m, 28H), 0.91–0.82 (m, 6H).

DMG-PEG-GalNAc: Briefly, NH2-PEG-N3 (11.8 mg, 0.046 mmol) and N-(3-Ammoniopropyl)-5-[3,4,6-tri-*O*-acetyl-2-acetamido-2-deoxy-β-D-glucopyranosyloxy]pentanamide trifluoroacetate (21) (69 mg, 0.035 mmol) were dissolved in 2 mL of DMF and stirred for 30 min at 0 °C.

Then, N,N′-Disuccinimidyl carbonate (100 mg, 0.162 mmol) was added at 0 °C and stirred overnight at room temperature (RT). The resulting mixture was concentrated and dissolved in triethylamine/methanol/water (1/1/1 *v*/v/v), followed by an overnight reaction at RT. After that, the solution was concentrated and underwent a reaction with 3-(prop-2-yn-1-yloxy)propane-1,2-diyl ditetradecanoate (44, 45) (55 mg, 0.10 mmol), utilizing CuI (10 mg, 0.05 mmol) and DIEA (26 mg, 0.2 mmol) catalysts, maintained at RT overnight. The yielded DMG-PEG-GalNAc (yellow solid, 45 mg) was purified by Prep-HPLC and characterized by ^{1}H NMR (400 MHz, Chloroform-*d*). *m/z* cal'd = 2977.9 ± 44.0, found 994.0 ± n*14.7(1/3 M + H+), 999.4 ± n*14.7 [(M + NH4++2H+)/3].

4.4. Preparation of @LNP and @LNP-GNc encapsulating mRNA and siRNA

Ionizable lipid (AA3-Dlin), DSPC, cholesterol, and PEG lipid (DMG-PEG or DMG-PEG-GalNAc) were diluted in ethanol and mixed at molar ratios of 47.5:10:40.7:1.8 [37]. mRNA encoding luciferase or IL-27 was diluted in sodium acetate buffer (pH 4.0, 10 mM). The ethanol phase and sodium acetate phase were loaded into two different syringes at a fixed N:P ratio of 6:1, respectively. The two phases were mixed in a microfluidic device (Herringbone Mixer Chip, LabSmith) at a total flow rate of 4 mL/min with a flow rate ratio of 3:1 (aqueous:organic). The resulting solution was incubated on ice for 20 min and then dialyzed against PBS (pH 7.4) for 4 h to form stable mRNA LNPs. The fresh LNP formulations were concentrated or diluted with PBS to an appropriate concentration for studies. DMG-PEG-GalNAc was incorporated into the ethanol phase at a molar ratio of 2.5 %. DiR dye was solubilized in ethanol and incorporated into LNPs at a molar ratio of 1 %, and dyed LNP samples were incubated for 1 h prior to dialysis.

4.5. Physical characterization of LNP formulations

The hydrodynamic diameter of LNP formulations was measured by Dynamic Light Scattering (DLS) on a Zetasizer HSIII (Malvern). The morphology of LNPs was characterized by Transmission Electron Microscopy (JEM-F200 TEM). mRNA encapsulation efficiency was determined by a Quant-it™ RiboGreen RNA Assay Kit (Invitrogen, USA). The total and free mRNA content were determined by dispersing LNPs in 1× TE buffer with or without the 2 % Triton X-100, respectively. A series of RNA standard solutions and LNP samples were incubated with RiboGreen reagents (1:200 dilution) for 5 min, and the fluorescence intensity was measured with a microplate reader (excitation/emission: 480/520 nm, Tecan, Switzerland).

4.6. Cell culture and transfection

Hepa1–6 cell lines were obtained from the American Type Culture Collection (ATCC). All cells were cultured in Dulbecco's modified Eagle's medium (DMEM) containing 10 % FBS, 100 units/mL penicillin, and 100 mg/mL streptomycin. Cells were grown in a humidified atmosphere with 5 % CO2 at 37 °C.

For in vitro transfection, 300 ng mRNA was encapsulated in LNPs as described above. The formulated mixtures were added into a well of a 48-well plate containing 300 mL medium. At predetermined time points after transfection, the cells or supernatants were collected for further assays.

4.7. Cellular uptake analysis

Hepa1–6 cells were seeded on glass slides overnight, followed by transfection with Luciferase *mLuc-*^{FITC}*LNPs* for 0.5, 2, or 4 h. The fluorescence images were acquired with a Keyence BZ-100× inverted microscope with a FITC filter lens.

4.8. In vivo imaging and biodistribution

In vivo luciferase distribution of *mLuc@LNP* and *mLuc@LNP-GNc* were studied in healthy B57BL/6 mice to evaluate biodistribution after intravenous administration. Briefly, mice were intravenously injected with mLuc loaded LNPs at a dose of 3 mg mLuc per mouse. 15 min prior to imaging timepoints, mice were intraperitoneally injected with 100 μL of D-Luciferin potassium salt bioluminescent substrate (15 mg/mL in PBS) and imaged on an in vivo imaging system (IVIS, PerkinElmer). Luminescence intensity was quantified using Living Image Software (PerkinElmer).

4.9. Animals DIO mice models, and in vivo therapeutic studies

All animal studies were approved by the Institutional Animal Care and Use Committee (IACUC) at Rutgers University. C57BL/6 J male mice aged 6–8 weeks were purchased from the Jackson Laboratory and housed in a temperature-controlled environment on a 12-h light cycle with free access to food and sterile water. The DIO model was established by feeding mice exclusively on HFD (TD06414, Teklad, 60 kcal from fat) for 5 weeks prior to treatment, and maintained on HFD during treatment for a total of 8 weeks.

For in vivo therapeutic studies, mice were intravenously injected into the lateral tail vein with different formulations twice a week for a period of 3 weeks ($n = 5$ per treatment group). The mice were sacrificed within 3 days after the final treatment, and blood as well as tissue samples were weighed, measured, and harvested for subsequent analysis.

4.10. Glucose tolerance test

Mice were fasted overnight, and glucose (1 g/kg) was administered intraperitoneally (i.p.), and the blood glucose levels were collected via tail vein nick, and measured at 0 min, 30 min, 60 min, 90 min and 120 min using OneTouch Ultra 2 glucose meter. The blood glucose level at 0 min was designated as the fasting glucose level.

4.11. Insulin tolerance test

Mice were fasted overnight and i.p. injected with insulin (0.75 U kg − 1), blood glucose levels were collected via tail vein nick, and measured at 0 min, 15 min, 30 min, 45 min, 60 min, 75 min, 90 min and 120 min using OneTouch Ultra 2 glucose meter.

4.12. ELISA assays

Serum assays using the ELISA kits for mouse IL-27 (BMS6024, ThermoFisher), Mouse leptin (EZML-82 K, MilliporeSigma), Mouse adiponectin (EZMADP-60 K, MilliporeSigma) and Rat/Mouse insulin (EZRMI-13 K, MilliporeSigma) were performed according to the manufacturer protocols.

4.13. Colorimetric assays

Serum assays using colorimetric assay kits for Free Fatty Acid (MAK466, MilliporeSigma) Triglyceride Colorimetric Assay Kit (10010303, Cayman Chemical) Cholesterol Quantitation Kit (MAK043-1KT, MilliporeSigma) were performed according to the manufacturer's protocols.

4.14. Histological analysis

Epididymal white adipose (eWAT), subcutaneous inguinal white adipose (SCW), and interscapular brown adipose (BAT) tissues were collected from mice for analysis. Adipose tissue samples were fixed overnight in 10 % neutral buffered formalin, dehydrated, and cleared prior to embedding in paraffin. Tissues were sliced into 5 μm sections on

a microtome (Leica), plated on SuperFrost Plus slides, deparaffinized and rehydrated prior to staining with H&E using standard protocols for each. Liver and organ tissues were fresh frozen embedded in OCT. Organ tissues were sliced into 8 um sections using a cryostat (Leica) and collected on SuperFrost Plus slides prior to H&E, and Oil Red O staining using standard protocols for each. Lipid droplet percent area and mean adipocyte areas for eWAT and SCW tissue were quantified by ImageJ (version 1.53 M, NIH) with the Adipocytes tools plugin. All images were observed under an optical microscope (Keyence, BZX-100).

4.15. Immunohistochemistry

IHC for UCP-1 was performed using rabbit specific HRP/DAB Detection IHC Kit (ab64261, Abcam) according to the manufacturers protocol. Briefly, sections were processed by heat activated epitope retrieval in 6.0 pH Tris-Citrate buffer overnight at 60C, blocked with hydrogen peroxidase and protein block, incubated with anti-UCP-1 (ab209483, Abcam), then treated with Streptavidin peroxidase followed by DAB chromogen, and counterstained by Hematoxylin. IHC staining percent area was quantified using ImageJ software. All images were observed under an optical microscope (Keyence, BZX-100).

4.16. Quantitative Real-Time PCR

Total RNA was extracted from tissue with Trizol (Invitrogen), purified with RNA Clean & Concentrator (Zymo), and quantified using a Nanodropp 2000 ultraviolet-visible spectrophotometer (ThermoFisher Scientific). cDNA was prepared by reverse transcription PCR using Superscript IV MasterMix (ThermoFisher). 100 ng of cDNA was amplified on QuantStudio 3 Real-Time PCR System (Applied Biosystems) using PowerUp SYBR qPCR Master Mix (ThermoFisher). The primer sequences for the qRT-PCR reactions are listed in Supplementary Table 1. GAPDH served as the endogenous reference, and the data were analyzed using the $2^{-\Delta\Delta}$CT method.

4.17. Western blotting

Total protein was extracted from liver and adipose tissues in RIPA lysis buffer with protease and phosphatase inhibitor cocktail (Sigma). The protein concentration was measured using a Pierce BCA protein assay kit (ThermoFisher). Then, the protein solution was mixed with 4× Laemmli sample buffer (Bio-Rad) and heated at 95 °C for 5 min. The samples were separated by SDS-polyacrylamide gel electrophoresis and transferred to polyvinylidene fluoride membrane (Millipore). The membranes were blocked with 5 % BSA in TBST buffer for 1 h and then incubated with primary antibodies overnight at 4 °C. The membranes were washed with TBST and further incubated with secondary antibodies for 1.5 h at room temperature, followed by detection using Western Blotting Luminol Reagent (SantaCruz). Primary antibodies were rabbit anti-PGC-1α (1:2000, Abcam), rabbit anti-PPARα (1:2000, Abcam), rabbit anti-UCP-1 (1:2000, Abcam), rabbit anti-GAPDH (1:10000, Abcam), goat anti-IL27 (1:2000, RD Systems), goat anti-DPP-4 (1:2000, RD Systems). Secondary antibodies were Chicken anti-goat IgG (1:5000, RD Systems), Goat anti-rabbit IgG (1:5000, Abcam). ImageJ software was used for optical density analysis.

4.18. Statistical analysis

All statistical data are analyzed by GraphPad Prism 10.2.3 software, and results are presented as means ± standard error (SEM). One-way analysis of variance (ANOVA) with post hoc Tukey test was employed to determine differences between groups. Two-way analysis of variance (ANOVA) with post hoc Tukey test was employed to determine differences between groups and adipose tissue weight. Two-way analysis of variance (ANOVA) with repeated measures and post hoc Tukey test was employed to determine differences between groups and bodyweight over time. A P-value <0.05 was considered statistically significant, whereas non-significant (ns) is indicated for values greater than 0.05.

CRediT authorship contribution statement

William Stewart: Writing – review & editing, Writing – original draft, Methodology, Investigation, Formal analysis, Data curation, Conceptualization. **Bin Hu:** Writing – review & editing. **Fengqiao Li:** Conceptualization. **Jia Huang:** Writing – review & editing. **Zhixiang Liu:** Formal analysis. **Chenshuang Zhang:** Writing – review & editing. **Maoping Tang:** Writing – review & editing. **Xue-Qing Zhang:** Writing – review & editing, Formal analysis, Conceptualization. **Xiaoyang Xu:** Writing – review & editing, Writing – original draft, Formal analysis, Conceptualization.

Funding

X.X. acknowledges funding from National Science Foundation (2001606). This research is also supported by the Gustavus and Louise Pfeiffer Research Foundation Award. X.-Q. Z. acknowledges funding from the National Key Research and Development Program of China (2023YFC2606003), "Open Competition to Select the Best Candidates" Key Technology Program for Nucleic Acid Drugs of NCTIB (grant no. NCTIB2022HS02002), the Natural Science Foundation of Shanghai (23ZR1427600), the Program of Shanghai Frontiers Science Center of Drug Target Identification and Delivery (ZXWH2170101), the National Science Foundation (2001606).

Declaration of competing interest

The authors declare no competing interests.

Appendix A. Supplementary data

Supplementary data to this article can be found online at https://doi.org/10.1016/j.jconrel.2025.113857.

Data and materials availability

All data associated with this study are present in the manuscript or the Supplementary Materials or is available upon request. Figure images created in BioRender. Stewart, W. (2025) https://BioRender.com/n12u516.

References

[1] Products - Data Briefs - Number 508, 2024, https://doi.org/10.15620/cdc/159281.
[2] Z.J. Ward, S.N. Bleich, A.L. Cradock, J.L. Barrett, C.M. Giles, C. Flax, M.W. Long, S. L. Gortmaker, Projected U.S, State-level prevalence of adult obesity and severe obesity, N. Engl. J. Med. 381 (25) (2019) 2440–2450, https://doi.org/10.1056/NEJMsa1909301.
[3] C. Koliaki, M. Dalamaga, S. Liatis, Update on the obesity epidemic: after the sudden rise, is the upward trajectory beginning to flatten? Curr. Obes. Rep. 12 (4) (2023) 514–527, https://doi.org/10.1007/s13679-023-00527-y.
[4] A. Elmaleh-Sachs, J.L. Schwartz, C.T. Bramante, J.M. Nicklas, K.A. Gudzune, M. Jay, Obesity Management in Adults A Review, JAMA 330 (20) (2023) 2000, https://doi.org/10.1001/jama.2023.19897.
[5] V. Rakhra, S.L. Galappaththy, S. Bulchandani, P.K. Cabandugama, Obesity and the Western diet: how we got here, Mo. Med. 117 (6) (2020) 536.
[6] K. Uneda, Y. Kawai, T. Yamada, S. Kinguchi, K. Azushima, T. Kanaoka, Y. Toya, H. Wakui, K. Tamura, Systematic review and Meta-analysis for prevention of cardiovascular complications using GLP-1 receptor agonists and SGLT-2 inhibitors in obese diabetic patients, Sci. Rep. 11 (1) (2021) 10166, https://doi.org/10.1038/s41598-021-89620-7.
[7] S. Ansari, B. Khoo, T. Tan, Targeting the incretin system in obesity and type 2 diabetes mellitus, Nat. Rev. Endocrinol. 20 (8) (2024) 447–459, https://doi.org/10.1038/s41574-024-00979-9.
[8] J.J. Holst, The incretin system in healthy humans: the role of GIP and GLP-1, Metabolism 96 (2019) 46–55, https://doi.org/10.1016/j.metabol.2019.04.014.
[9] J.J. Holst, N.J.W. Albrechtsen, M.M. Rosenkilde, C.F. Deacon, Physiology of the incretin hormones, GIP and GLP-1—Regulation of release and posttranslational

modifications, in: Comprehensive Physiology, John Wiley & Sons, Ltd, 2019, pp. 1339–1381, https://doi.org/10.1002/cphy.c180013.
[10] M.A. Nauck, J.J. Meier, Incretin hormones: their role in health and disease, Diabetes Obes. Metab. 20 (S1) (2018) 5–21, https://doi.org/10.1111/dom.13129.
[11] Z. Zheng, Y. Zong, Y. Ma, Y. Tian, Y. Pang, C. Zhang, J. Gao, Glucagon-like Peptide-1 receptor: mechanisms and advances in therapy, Signal Transduct. Target. Ther. 9 (1) (2024) 1–29, https://doi.org/10.1038/s41392-024-01931-z.
[12] A.M. Jastreboff, L.J. Aronne, N.N. Ahmad, S. Wharton, L. Connery, B. Alves, A. Kiyosue, S. Zhang, B. Liu, M.C. Bunck, A. Stefanski, Tirzepatide once weekly for the treatment of obesity, N. Engl. J. Med. 387 (3) (2022) 205–216, https://doi.org/10.1056/NEJMoa2206038.
[13] M.A. Nauck, D'Alessio, D. A., Tirzepatide, a dual GIP/GLP-1 receptor co-agonist for the treatment of type 2 diabetes with unmatched effectiveness regrading Glycaemic control and body weight reduction, Cardiovasc. Diabetol. 21 (1) (2022) 169, https://doi.org/10.1186/s12933-022-01604-7.
[14] F. Zhao, Q. Zhou, Z. Cong, K. Hang, X. Zou, C. Zhang, Y. Chen, A. Dai, A. Liang, Q. Ming, M. Wang, L.-N. Chen, P. Xu, R. Chang, W. Feng, T. Xia, Y. Zhang, B. Wu, D. Yang, L. Zhao, H.E. Xu, M.-W. Wang, Structural insights into multiplexed pharmacological actions of Tirzepatide and peptide 20 at the GIP, GLP-1 or glucagon receptors, Nat. Commun. 13 (1) (2022) 1057, https://doi.org/10.1038/s41467-022-28683-0.
[15] J. Rosenstock, J. Frias, A.M. Jastreboff, Y. Du, J. Lou, S. Gurbuz, M.K. Thomas, M. L. Hartman, A. Haupt, Z. Milicevic, T. Coskun, Retatrutide, a GIP, GLP-1 and glucagon receptor agonist, for people with type 2 diabetes: A randomised, double-blind, placebo and active-controlled, parallel-group, phase 2 trial conducted in the USA, Lancet 402 (10401) (2023) 529–544, https://doi.org/10.1016/S0140-6736(23)01053-X.
[16] D. Do, T. Lee, S.K. Peasah, C.B. Good, A. Inneh, U. Patel, GLP-1 receptor agonist discontinuation among patients with obesity and/or type 2 diabetes, JAMA Netw. Open 7 (5) (2024) e2413172, https://doi.org/10.1001/jamanetworkopen.2024.13172.
[17] R. Nogueiras, M.A. Nauck, M.H. Tschöp, Gut hormone co-agonists for the treatment of obesity: from bench to bedside, Nat. Metab. 5 (6) (2023) 933–944, https://doi.org/10.1038/s42255-023-00812-z.
[18] T. Coskun, S. Urva, W.C. Roell, H. Qu, C. Loghin, J.S. Moyers, L.S. O'Farrell, D. A. Briere, K.W. Sloop, M.K. Thomas, V. Pirro, D.B. Wainscott, F.S. Willard, M. Abernathy, L. Morford, Y. Du, C. Benson, R.E. Gimeno, A. Haupt, Z. Milicevic, LY3437943, a novel triple glucagon, GIP, and GLP-1 receptor agonist for glycemic control and weight loss: from discovery to clinical proof of concept, Cell Metab. 34 (9) (2022) 1234–1247.e9, https://doi.org/10.1016/j.cmet.2022.07.013.
[19] C.I. Colino, J.M. Lanao, C. Gutierrez-Millan, Targeting of hepatic macrophages by therapeutic nanoparticles, Front. Immunol. 11 (2020) 218, https://doi.org/10.3389/fimmu.2020.00218.
[20] L.N. Kasiewicz, S. Biswas, A. Beach, H. Ren, C. Dutta, A.M. Mazzola, E. Rohde, A. Chadwick, C. Cheng, S.P. Garcia, S. Iyer, Y. Matsumoto, A.V. Khera, K. Musunuru, S. Kathiresan, P. Malyala, K.G. Rajeev, A.M. Bellinger, GalNAc-lipid nanoparticles enable non-LDLR dependent hepatic delivery of a CRISPR Base editing therapy, Nat. Commun. 14 (1) (2023) 2776, https://doi.org/10.1038/s41467-023-37465-1.
[21] Y. Zhou, P. Teng, N.T. Montgomery, X. Li, W. Tang, Development of Triantennary N-Acetylgalactosamine conjugates as degraders for extracellular proteins, ACS Cent. Sci. 7 (3) (2021) 499–506, https://doi.org/10.1021/acscentsci.1c00146.
[22] K. Fitzgerald, S. White, A. Borodovsky, B.R. Bettencourt, A. Strahs, V. Clausen, P. Wijngaard, J.D. Horton, J. Taubel, A. Brooks, C. Fernando, R.S. Kauffman, D. Kallend, A. Vaishnaw, A. Simon, A highly durable RNAi therapeutic inhibitor of PCSK9, N. Engl. J. Med. 376 (1) (2016) 41, https://doi.org/10.1056/NEJMoa1609243.
[23] Q. Wang, D. Li, G. Cao, Q. Shi, J. Zhu, M. Zhang, H. Cheng, Q. Wen, H. Xu, L. Zhu, H. Zhang, R.J. Perry, O. Spadaro, Y. Yang, S. He, Y. Chen, B. Wang, G. Li, Z. Liu, C. Yang, X. Wu, L. Zhou, Q. Zhou, Z. Ju, H. Lu, Y. Xin, X. Yang, C. Wang, Y. Liu, G. I. Shulman, V.D. Dixit, L. Lu, H. Yang, R.A. Flavell, Z. Yin, IL-27 Signalling promotes adipocyte thermogenesis and energy expenditure, Nature 600 (7888) (2021) 314–318, https://doi.org/10.1038/s41586-021-04127-5.
[24] Y. Yang, H. Liu, D. Liu, Preventing high-fat diet-induced obesity and related metabolic disorders by hydrodynamic transfer of Il-27 gene, Int. J. Obes. 47 (5) (2023) 413–421, https://doi.org/10.1038/s41366-023-01293-6.
[25] T. Akimoto, S.C. Pohnert, P. Li, M. Zhang, C. Gumbs, P.B. Rosenberg, R.S. Williams, Z. Yan, Exercise stimulates Pgc-1α transcription in skeletal muscle through activation of the P38 MAPK pathway*, J. Biol. Chem. 280 (20) (2005) 19587–19593, https://doi.org/10.1074/jbc.M408862200.
[26] P.J. Fernandez-Marcos, J. Auwerx, Regulation of PGC-1α, a nodal regulator of mitochondrial biogenesis, Am. J. Clin. Nutr. 93 (4) (2011) 884S–890S, https://doi.org/10.3945/ajcn.110.001917.
[27] H. Liang, W.F. Ward, PGC-1α: A key regulator of energy metabolism, Adv. Physiol. Educ. 30 (4) (2006) 145–151, https://doi.org/10.1152/advan.00052.2006.
[28] D.E. Moller, J.P. Berger, Role of PPARs in the regulation of obesity-related insulin sensitivity and inflammation, Int. J. Obes. 27 (S3) (2003) S17–S21, https://doi.org/10.1038/sj.ijo.0802494.
[29] P. Tontonoz, E. Hu, B.M. Spiegelman, Stimulation of Adipogenesis in fibroblasts by PPARγ2, a lipid-activated transcription factor, Cell 79 (7) (1994) 1147–1156, https://doi.org/10.1016/0092-8674(94)90006-X.
[30] M. Leiva, N. Matesanz, M. Pulgarín-Alfaro, I. Nikolic, G. Sabio, Uncovering the role of P38 family members in adipose tissue physiology, Front. Endocrinol. 11 (2020) 572089, https://doi.org/10.3389/fendo.2020.572089.
[31] D.S. Ghorpade, L. Ozcan, Z. Zheng, S.M. Nicoloro, Y. Shen, E. Chen, M. Blüher, M. P. Czech, I. Tabas, Hepatocyte-secreted DPP4 in obesity promotes adipose inflammation and insulin resistance, Nature 555 (7698) (2018) 673–677, https://doi.org/10.1038/nature26138.
[32] D. Lamers, S. Famulla, N. Wronkowitz, S. Hartwig, S. Lehr, D.M. Ouwens, K. Eckardt, J.M. Kaufman, M. Ryden, S. Müller, F.-G. Hanisch, J. Ruige, P. Arner, H. Sell, J. Eckel, Dipeptidyl peptidase 4 is a novel Adipokine potentially linking obesity to the metabolic syndrome, Diabetes 60 (7) (2011) 1917–1925, https://doi.org/10.2337/db10-1707.
[33] R. Mentlein, Dipeptidyl-peptidase IV (CD26)-role in the inactivation of regulatory peptides, Regul. Pept. 85 (1) (1999) 9–24, https://doi.org/10.1016/S0167-0115(99)00089-0.
[34] J. Malzahn, A. Kastrenopoulou, I. Papadimitriou-Olivgeri, D.J. Papachristou, J. M. Brown, U. Oppermann, N.A. Athanasou, Immunophenotypic expression of UCP1 in Hibernoma and other adipose/non adipose soft tissue tumours, Clin. Sarcoma Res. 9 (2019) 8, https://doi.org/10.1186/s13569-019-0118-1.
[35] S. Kajimura, M. Saito, A new era in Brown adipose tissue biology: molecular control of Brown fat development and energy homeostasis, Annu. Rev. Physiol. 76 (2014) 225–249, https://doi.org/10.1146/annurev-physiol-021113-170252.
[36] S. Heinonen, R. Jokinen, A. Rissanen, K.H. Pietiläinen, White adipose tissue mitochondrial metabolism in health and in obesity, Obes. Rev. Off. J. Int. Assoc. Study Obes. 21 (2) (2020) e12958, https://doi.org/10.1111/obr.12958.
[37] Z. Li, X.-Q. Zhang, W. Ho, F. Li, M. Gao, X. Bai, X. Xu, Enzyme-catalyzed one-step synthesis of Ionizable cationic lipids for lipid nanoparticle-based mRNA COVID-19 vaccines, ACS Nano 16 (11) (2022) 18936–18950, https://doi.org/10.1021/acsnano.2c07822.
[38] M.-S. Popoviciu, L. Păduraru, G. Yahya, K. Metwally, S. Cavalu, Emerging role of GLP-1 agonists in obesity: A comprehensive review of randomised controlled trials, Int. J. Mol. Sci. 24 (13) (2023) 10449, https://doi.org/10.3390/ijms241310449.
[39] Y. Xue, X. Xu, X.-Q. Zhang, O.C. Farokhzad, R. Langer, Preventing diet-induced obesity in mice by adipose tissue transformation and angiogenesis using targeted nanoparticles, Proc. Natl. Acad. Sci. 113 (20) (2016) 5552–5557, https://doi.org/10.1073/pnas.1603840113.
[40] M.E.J. Lean, D. Malkova, Altered gut and adipose tissue hormones in overweight and obese individuals: cause or consequence? Int. J. Obes. 40 (4) (2016) 622–632, https://doi.org/10.1038/ijo.2015.220.